Mathematical Biosciences and Engineering

https://www.aimspress.com/journal/mbe

MBE, 21(5): 6042–6076.
DOI: 10.3934/mbe.2024266
Received: 05 April 2024
Revised: 13 May 2024
Accepted: 20 May 2024
Published: 24 May 2024

Research article

New insights into the effects of small permanent charge on ionic flows: A higher order analysis

Hamid Mofidi[1,2,*]

[1] Beijing Institute of Mathematical Sciences and Applications (BIMSA), Beijing 101408, China
[2] Yau Mathematical Sciences Center, Tsinghua University, Beijing 100084, China

* **Correspondence:** E-mail: h.mofidi@bimsa.cn.

Abstract: This study investigated how permanent charges influence the dynamics of ionic channels. Using a quasi-one-dimensional classical Poisson–Nernst–Planck (PNP) model, we investigated the behavior of two distinct ion species—one positively charged and the other negatively charged. The spatial distribution of permanent charges was characterized by zero values at the channel ends and a constant charge Q_0 within the central region. By treating the classical PNP model as a boundary value problem (BVP) for a singularly perturbed system, the singular orbit of the BVP depended on Q_0 in a regular way. We therefore explored the solution space in the presence of a small permanent charge, uncovering a systematic dependence on this parameter. Our analysis employed a rigorous perturbation approach to reveal higher-order effects originating from the permanent charges. Through this investigation, we shed light on the intricate interplay among boundary conditions and permanent charges, providing insights into their impact on the behavior of ionic current, fluxes, and flux ratios. We derived the quadratic solutions in terms of permanent charge, which were notably more intricate compared to the linear solutions. Through computational tools, we investigated the impact of these quadratic solutions on fluxes, current-voltage relations, and flux ratios, conducting a thorough analysis of the results. These novel findings contributed to a deeper comprehension of ionic flow dynamics and hold potential implications for enhancing the design and optimization of ion channel-based technologies.

Keywords: permanent charge; ionic flows; PNP; flux ratios; I-V relations

1. Introduction

Ion channels, proteins within cell membranes, are vital for cell communication, signal transformation, and coordinated activities [1, 2]. They are defined by their shape and permanent charge. These channels typically resemble cylinders, with amino acid side chains concentrated in a short and narrow region. Acidic side chains contribute negative charges, while basic side chains add positive charges, determining the channel's permanent charge. Channel structures selectively permit specific ions and ease their diffusion across cell membranes [3–7].

Permeation and selectivity properties of ion channels are currently derived mainly from experimentally measured current-voltage (I-V) relations [2, 5, 8, 9]. While individual fluxes convey more detailed information, they are costly and difficult to measure [6, 10]. The I-V relation reflects the channel structure's response to ionic fluxes but is influenced by boundary conditions that drive ionic transport [11, 12]. This multi-scale nature, with various physical parameters, grants the system great flexibility and diverse behaviors—a hallmark of natural devices [3]. However, this complexity also poses challenges in extracting meaningful insights from experimental data, especially given the limitations in observing internal dynamics.

The Poisson-Nernst-Planck (PNP) model stands out as one of the most commonly utilized mathematical frameworks for studying ion channels [13–21]. This model takes into account the interplay between structural characteristics and physical parameters, and researchers have extensively examined it using a geometric singular perturbation (GSP) approach [22, 23]. Through the application of this approach, the PNP model can be simplified into an algebraic system referred to as the governing system. Analyzing this governing system unveils crucial properties of ion channels, providing valuable insights for informed design and optimization across various applications [24, 25].

The effects of permanent charge on ionic flows have been investigated by several studies using the PNP model, with both analytical and numerical methods [10, 26–28]. Liu et al. [10, 27] examined the flux ratios and ion channel structures via PNP, and analyzed how they influence the fluxes, boundary concentrations, and electric potentials of the system. Other papers explored the reversal potential and permanent charge under unequal diffusion coefficients, and derived universal properties of the system [29–33] or numerically studied the permanent charge effects on flux ratios, revealing new phenomena and qualitative changes [34, 35]. These studies enhance the understanding of the channel geometry and the role of permanent charge in ion channel dynamics.

Given the complex and multi-scale nature of the problem at hand, a comprehensive understanding of the interactions between permanent charges and boundary conditions cannot solely rely on analytical methods, especially across varying magnitudes of permanent charges. Therefore, this study adopts a combined approach of analytical insights and numerical methods to delve deeper into how permanent charges influence ionic flows in the presence of electric potentials. Leveraging previous analytical work, particularly from studies such as [16, 36], which investigated flux ratios under different conditions, the focus narrows down to the flux ratio introduced in [27], examining its dependencies on permanent charges and electric potentials.

The methodology integrates rigorous analysis and numerical simulations to explore the impact of permanent charges on individual fluxes within fixed-shape open channels. Rigorous analysis uncovers essential biological properties and classifies distinct behaviors across various physical domains, especially in limiting or ideal scenarios. Conversely, numerical simulations extend these analytical findings into realistic parameter ranges, often unveiling additional phenomena. This approach allows a deeper dive into the intricacies of permanent charge effects, expanding upon previous analyses based on the PNP framework, which have revealed intriguing phenomena related to small permanent charges [16].

For the numerical simulations, Python along with the Numpy and Matplotlib libraries [37] are utilized. The computational code used in this study is publicly accessible through the author's GitHub repository at https://github.com/Hamid-Mofidi/PNP/tree/main/Q2contribution. This open access repository encourages collaboration and facilitates knowledge sharing among researchers interested in this field.

In this manuscript, we revisit the zeroth and first order solutions in permanent charge, as outlined in [16], to pave the way for higher-order analyses. The new findings and highlights of our studies in this manuscript are as follows:

(a) We derive analytical expressions for the intricate second order solutions, which are elaborated in Section 3.2 and form the backbone of our study.
(b) We study the effect of permanent charge and boundary concentrations on fluxes and I-V relations, estimate error and assess nonlinear effects for fluxes (explained in Section 4).
(c) In Section 5, we explore the higher order impact of permanent charge on flux ratios and analyze their dependencies on voltages and permanent charges.

In addition, the combination of our analytical (Section 3) and numerical investigations (Sections 4 and 5) shed light on both linear and quadratic solutions, providing novel insights and expanding our understanding beyond existing frameworks. These results serve as the foundation for further exploration and analysis in this study.

The paper follows this structure: Section 2 introduces the classical PNP model for ion channels and establishes a quasi-one-dimensional electro-diffusion model in Section 2.1, considering two types of ions with different charges and a simple distribution of permanent charge. Section 2.2 transforms the model into a dimensionless form for simplified analysis. Section 2.3 presents the governing system for the boundary value problem (BVP). In Section 3, the singular solutions in the presence of small permanent charge are analyzed, exploring higher-order effects. Sections 3.1 and 3.2 respectively delve into the zeroth, first, and second order solutions and their implications for system behavior. Notably, Section 3.2 introduces new analytical results for the second order solutions in Q_0. Section 4 provides computational outcomes for the first and second order solutions in Q_0 and numerically investigates the impact of permanent charge on fluxes and I-V relations, revealing the intricate interplay between permanent charge, boundary conditions, and channel geometry. Sections 4.1 and 4.2 respectively focus on the first and second order effects. In Section 5, we study the higher order effects of small positive permanent charges on flux ratios. Finally, Section 6 concludes the manuscript, summarizing the main results, discussing implications, and suggesting directions for future research.

2. Classical PNP systems for ion channels: Setup and key results

PNP systems, essential for studying ionic flows, originate from molecular dynamic models [38], Boltzmann equations [39], and variational principles [40, 41]. Advanced coupling with Navier–Stokes equations [42–44] and rigorous establishment of the Onsager reciprocal law [45] offer sophisticated insights, striking a balance between accuracy and analytical/computational challenges, supported by reviews and model comparisons [46, 47].

Building upon this foundation, we further streamline PNP models, especially for ion channels with narrow cross-sections relative to lengths, resulting in quasi-one-dimensional models [48]. This reduction yields quasi-one-dimensional models [48], with rigorous justification provided in [49]. The streamlined approach addresses both accuracy and analytical/computational challenges.

This section provides a detailed exposition of our mathematical model for ionic flows, focusing on the essential setup and key results. Specifically, we explore a quasi-one-dimensional PNP model that characterizes ion transport within a confined channel featuring a permanent charge. To ensure clarity in our subsequent analysis, we introduce notation and assumptions consistently used throughout the paper. Moreover, we review relevant findings from previous literature, such as [14, 18], serving as crucial foundations for our contributions outlined in the following sections.

Remark 2.1. *The time-dependent PNP model has been discussed in [14]. Equation (2.1) in the following is selected based on two primary reasons: First, the one-dimensional system offers simplicity. Second, if the one-dimensional limiting system maintains structural stability, the dynamics of the three-dimensional system mirror those of the one-dimensional counterpart. Verification of structural stability follows a well-established framework, albeit nontrivial. Therefore, understanding the behavior of the steady-state in the limiting one-dimensional system serves as a pivotal step in this context.*

2.1. A quasi-one-dimensional PNP model

Our analysis is based on a quasi-one-dimensional PNP model first proposed in [48] and, for a special case, rigorously justified in [49]. For a mixture of n ion species, a quasi-one-dimensional PNP model is

$$\begin{aligned} &\frac{1}{A(X)}\frac{d}{dX}\Big(\varepsilon_r(X)\varepsilon_0 A(X)\frac{d\Phi}{dX}\Big) = -e_0\Big(\sum_{s=1}^{n} z_s C_s + Q(X)\Big),\\ &\frac{d\mathcal{J}_k}{dX} = 0, \quad -\mathcal{J}_k = \frac{1}{k_B T}\mathcal{D}_k(X)A(X)C_k\frac{d\mu_k}{dX}, \quad k = 1, 2, \cdots, n, \end{aligned} \tag{2.1}$$

where $X \in [a_0, b_0]$ is the coordinate along the axis of the channel and baths of total length $b_0 - a_0$, $A(X)$ is the area of cross-section of the channel over the longitudinal location X, e_0 is the elementary charge, ε_0 is the vacuum permittivity, $\varepsilon_r(X)$ is the relative dielectric coefficient, $Q(X)$ is the permanent charge density, k_B is the Boltzmann constant, T is the absolute temperature, Φ is the electric potential, for the kth ion species, C_k is the concentration, z_k is the valence, $\mathcal{D}_k(X)$ is the diffusion coefficient, μ_k is the electrochemical potential, and $\mathcal{J}_k$ is the flux density.

Equipped with the system (2.1), a meaningful boundary condition for ionic flow through ion channels (see, [14] for reasoning) is, for $k = 1, 2, \cdots, n$,

$$\Phi(a_0) = \mathcal{V}, \;\; C_k(a_0) = \mathcal{L}_k > 0; \quad \Phi(b_0) = 0, \;\; C_k(b_0) = \mathcal{R}_k > 0. \tag{2.2}$$

In relation to typical experimental designs, the positions $X = a_0$ and $X = b_0$ are located in the baths separated by the channel and are locations for two electrodes that are applied to control or drive the ionic flow through the ion channel. An important measurement is the I-V (current-voltage) relation where, for fixed $\mathcal{L}_k$'s and $\mathcal{R}_k$'s, the current $\mathcal{I}$ depends on the transmembrane potential (voltage) $\mathcal{V}$ by $\mathcal{I} = \sum_{s=1}^{n} z_s\mathcal{J}_s(\mathcal{V})$.

Certainly, the relations of individual fluxes $\mathcal{J}_k$ with respect to $\mathcal{V}$ are more informative, but, measuring them experimentally is much more difficult [50]. Ideally, the experimental designs should not affect the intrinsic ionic flow properties so one would like to design the boundary conditions to meet the so-called electroneutrality $\sum_{s=1}^{n} z_s\mathcal{L}_s = 0 = \sum_{s=1}^{n} z_s\mathcal{R}_s$. The reason for this is that, otherwise, there will be sharp boundary layers which cause significant changes (large gradients) of the electric potential and concentrations near the boundaries so that a measurement of these values has nontrivial uncertainties. One smart design to remedy this potential problem is the "four-electrode-design": two 'outer electrodes' in the baths far away from the ends of the ion channel to provide the driving force and two 'inner electrodes' in the baths near the ends of the ion channel to measure the electric potential and the concentrations as the "real" boundary conditions for the ionic flow. At the inner electrodes locations, the electroneutrality conditions are reasonably satisfied, and hence, the electric potential and concentrations vary slowly and a measurement of these values would be robust. The cross-sectional area $A(X)$ generally exhibits the characteristic of being significantly smaller for X in the interval (a_0, b_0) (representing the neck region of the channel) compared to X outside the interval $[a_0, b_0]$.

2.2. Dimensionless form of the quasi-one-dimensional PNP model

The following rescaling or its variations have been widely used for the convenience of mathematical analysis [51, 52]. Let C_0 be a characteristic concentration of the ion solution. We now make a dimensionless rescaling of the variables in the system (2.1) as follows.

$$\begin{aligned}
&\varepsilon^2 = \frac{\varepsilon_r \varepsilon_0 k_B T}{e_0^2 (b_0 - a_0)^2 C_0},\ x = \frac{X - a_0}{b_0 - a_0},\ h(x) = \frac{A(X)}{(b_0 - a_0)^2},\ Q(x) = \frac{\mathcal{Q}(X)}{C_0},\\
&D(x) = \mathcal{D}(X),\ \phi(x) = \frac{e_0}{k_B T}\Phi(X),\ c_k(x) = \frac{C_k(X)}{C_0},\ J_k = \frac{\mathcal{J}_k}{(b_0 - a_0) C_0 \mathcal{D}_k}.
\end{aligned} \tag{2.3}$$

We assume C_0 is fixed but large so that the parameter ε is small. Note that $\varepsilon = \lambda_D/(b_0 - a_0)$, where λ_D is the Debye screening length. In terms of the new variables, the BVP (2.1) and (2.2) becomes

$$\begin{aligned}
&\frac{\varepsilon^2}{h(x)} \frac{d}{dx}\left(h(x)\frac{d\phi}{dx}\right) = -\sum_{s=1}^{n} z_s c_s - Q(x),\\
&\frac{dJ_k}{dx} = 0, \quad -J_k = \frac{1}{k_B T} D(x) h(x) c_k \frac{d\mu_k}{dx},
\end{aligned} \tag{2.4}$$

with boundary conditions at $x = 0$ and $x = 1$

$$\phi(0) = V,\ c_k(0) = L_k;\ \phi(1) = 0,\ c_k(1) = R_k, \tag{2.5}$$

where $V := \frac{e_0}{k_B T}\mathcal{V}$, $\quad L_k := \frac{\mathcal{L}_k}{C_0}$, $\quad R_k := \frac{\mathcal{R}_k}{C_0}$. The permanent charge $Q(x)$ is

$$Q(x) = \begin{cases} 0, & x \in (0, a) \cup (b, 1)\\ Q_0, & x \in (a, b), \end{cases} \tag{2.6}$$

where $0 < a = \frac{A - a_0}{a_1 - a_0} < b = \frac{B - a_0}{a_1 - a_0} < 1$. We will take the ideal component μ_k^{id} only for the electrochemical potential. In terms of the new variables, it becomes

$$\frac{1}{k_B T}\mu_k^{id}(x) = z_k \phi(x) + \ln c_k(x). \tag{2.7}$$

The ideal component $\mu_k^{id}(x)$ contains contributions of ion particles as point charges and ignores the ion-to-ion interaction. PNP models including ideal components are referred to as classical PNP models. Recall that the critical assumption is that ε is small. This assumption allows us to treat the BVP (2.4) with (2.5) as a singularly perturbed problem. A general framework for analyzing such singularly perturbed BVPs in PNP-type systems has been developed in prior works [14, 18] for classical PNP systems and in [34, 52, 53] for PNP systems with finite ion sizes.

A method described in [14] (expanded upon in [18]) addresses the connection issue within classical PNP models by breaking down the system into two subsystems: the fast and slow systems under limiting conditions. Leveraging the specific structures of the PNP system allows for the integration of these subsystems, resulting in the creation of a singular orbit as an initial approximation. Aligning slow and fast orbits gives rise to a set of algebraic equations governing these singular orbits. This study takes a direct approach using regular perturbation theory to derive singular orbits for small magnitudes of $|Q_0|$, complementing the broader methodology detailed in previous literature.

We now recall the result from [14], upon which our work will be based. For $n = 2$ with $z_1 > 0 > z_2$, the authors applied the GSP theory to construct the singular orbit of the BVP (2.4) and (2.5). The BVP is then reduced to a connecting problem: finding an orbit from $B_0 = \{(V, u, L_1, L_2, J_1, J_2, 0) :$ arbitrary $u, J_1, J_2\}$, to $B_1 = \{(0, u, R_1, R_2, J_1, J_2, 1) :$ arbitrary $u, J_1, J_2\}$.

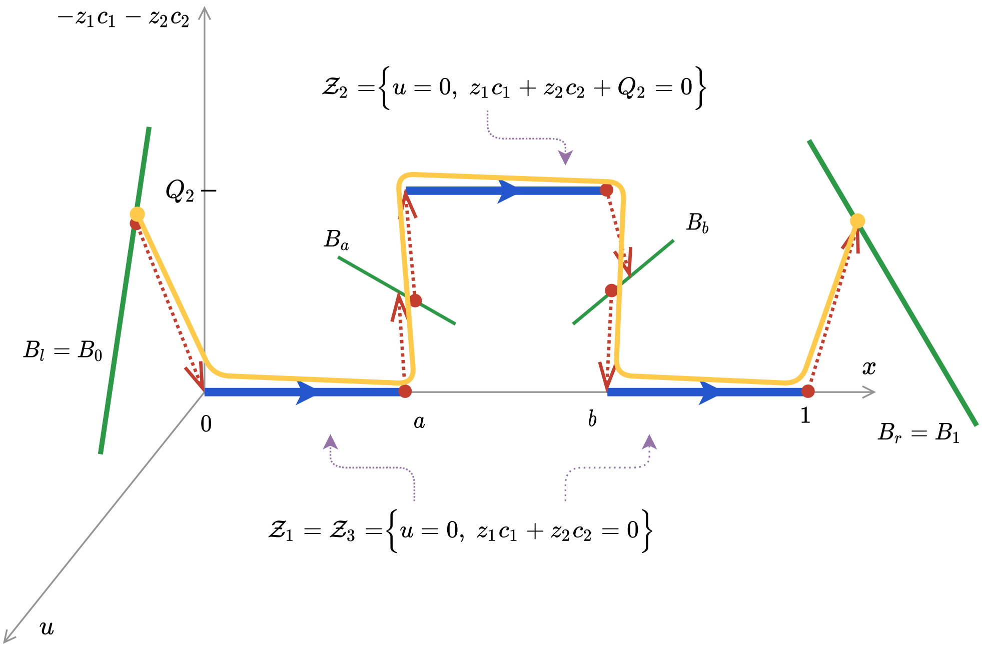

Figure 1. Illustration showing a singular connecting orbit projected onto the $(u; z_1c_1 + z_2c_2; x)$ space. The solid line represents the $O(\varepsilon)$ estimate of the connected problem, obtained using the Exchange Lemma (see [14, 22]), from the left boundary B_l to the right boundary B_r.

On each interval, a singular orbit typically consists of two singular layers and one regular layer:

(1) In view of the jumps of permanent charge $Q(x)$ at $x = a$ and $x = b$, the construction of singular orbits is split into three intervals $[0, a]$, $[a, b]$, $[b, 1]$, as depicted in Figure 1. To do so, one introduces (unknown) values of (ϕ, c_1, c_2) at $x = a$ and $x = b$:

$$\phi(a) = \phi^a,\ c_1(a) = c_1^a,\ c_2(a) = c_2^a;\quad \phi(b) = \phi^b,\ c_1(b) = c_1^b,\ c_2(a) = c_2^b. \tag{2.8}$$

These values then determine boundary conditions at $x = a$ and $x = b$ as $B_a = \{(\phi^a, u, c_1^a, c_2^a, J_1, J_2, a) :$ arbitrary $u, J_1, J_2\}$, and $B_b = \{(\phi^b, u, c_1^b, c_2^b, J_1, J_2, b) :$ arbitrary $u, J_1, J_2\}$. Consequently, there are six unknowns ϕ^a, ϕ^b, c_k^a, and c_k^b for $k = 1, 2$ that should be determined. On interval $[0,a]$, a singular orbit from B_0 to B_a consists of two singular layers located at $x=0$ and $x=a$, denoted as Γ_0^l and Γ_a^l, and one regular layer Λ_l. Furthermore, with the preassigned values ϕ^a, c_1^a, and c_2^a, the flux J_k^l and $u_l(a)$ are uniquely determined so that $(\phi^a, u_l(a), c_1^a, c_2^a, J_1^l, J_2^l, a) \in B_a$.

(2) On interval $[a,b]$, a singular orbit from B_a to B_b consists of two singular layers located at $x=a$ and $x=b$, denoted as Γ_a^r and Γ_b^l, and one regular layer Λ_m. Furthermore, with the preassigned values (ϕ^a, c_1^a, c_2^a) and (ϕ^b, c_1^b, c_2^b), the flux J_k^m, $u_m(a)$ and $u_m(b)$ are uniquely determined so that $(\phi^a, u_m(a), c_1^a, c_2^a, J_1^m, J_2^m, a) \in B_a$ and $(\phi^b, u_m(b), c_1^b, c_2^b, J_1^m, J_2^m, b) \in B_b$.

(3) On interval $[b,1]$, a singular orbit from B_b to B_1 consists of two singular layers are located at $x=b$ and $x=1$, denoted as Γ_b^r and Γ_1^l, and one regular layer Λ_r. Furthermore, with the preassigned values ϕ^b, c_1^b, and c_2^b, the flux J_k^r and $u_r(b)$ are uniquely determined so that $(\phi^b, u_r(b), c_1^b, c_2^b, J_1^r, J_2^r, b) \in B_b$.

2.3. *Governing system for the BVP*

The matching conditions of the connecting problem in the previous section are

$$J_k^l = J_k^m = J_k^r \ \text{ for } \ k=1,2, \ u_l(a) = u_m(a) \ \text{ and } \ u_m(b) = u_r(b). \tag{2.9}$$

There are a total of six conditions, which are exactly the same number of unknowns preassigned in (2.8). Then, the singular connecting problem is reduced to *the governing system* (2.9) (see [14] for an explicit form of the governing system). More precisely,

$$\begin{aligned}
& z_1 c_1^a e^{z_1(\phi^a - \phi^{a,m})} + z_2 c_2^a e^{z_2(\phi^a - \phi^{a,m})} + Q_0 = 0, \\
& z_1 c_1^b e^{z_1(\phi^b - \phi^{b,m})} + z_2 c_2^b e^{z_2(\phi^b - \phi^{b,m})} + Q_0 = 0, \\
& \frac{z_2 - z_1}{z_2} c_1^{a,l} = c_1^a e^{z_1(\phi^a - \phi^{a,m})} + c_2^a e^{z_2(\phi^a - \phi^{a,m})} + Q_0(\phi^a - \phi^{a,m}), \\
& \frac{z_2 - z_1}{z_2} c_1^{b,r} = c_1^b e^{z_1(\phi^b - \phi^{b,m})} + c_2^b e^{z_2(\phi^b - \phi^{b,m})} + Q_0(\phi^b - \phi^{b,m}), \\
& J_1 = \frac{c_1^L - c_1^{a,l}}{H(a)}\Big(1 + \frac{z_1(\phi^L - \phi^{a,l})}{\ln c_1^L - \ln c_1^{a,l}}\Big) = \frac{c_1^{b,r} - c_1^R}{H(1) - H(b)}\Big(1 + \frac{z_1(\phi^{b,r} - \phi^R)}{\ln c_1^{b,r} - \ln c_1^R}\Big), \\
& J_2 = \frac{c_2^L - c_2^{a,l}}{H(a)}\Big(1 + \frac{z_2(\phi^L - \phi^{a,l})}{\ln c_2^L - \ln c_2^{a,l}}\Big) = \frac{c_2^{b,r} - c_2^R}{H(1) - H(b)}\Big(1 + \frac{z_2(\phi^{b,r} - \phi^R)}{\ln c_2^{b,r} - \ln c_2^R}\Big), \\
& \phi^{b,m} = \phi^{a,m} - (z_1 J_1 + z_2 J_2) y, \\
& c_1^{b,m} = e^{z_1 z_2 (J_1 + J_2) y} c_1^{a,m} - \frac{Q_0 J_1}{z_1(J_1 + J_2)}\Big(1 - e^{z_1 z_2 (J_1 + J_2) y}\Big), \\
& J_1 + J_2 = -\frac{(z_1 - z_2)(c_1^{a,m} - c_1^{b,m}) + z_2 Q_0 (\phi^{a,m} - \phi^{b,m})}{z_2(H(b) - H(a))},
\end{aligned} \tag{2.10}$$

where $y > 0$ is also unknown, and under electroneutrality boundary conditions $z_1L_1 = -z_2L_2 = L$ and $z_1R_1 = -z_2R_2 = R$,

$$\begin{aligned}
\phi^L =& V, \quad \phi^R = 0, \quad z_1c_1^L = -z_2c_2^L = L, \quad z_1c_1^R = -z_2c_2^R = R,\\
\phi^{a,l} =& \phi^a - \frac{1}{z_1 - z_2}\ln\frac{-z_2c_2^a}{z_1c_1^a}, \quad \phi^{b,r} = \phi^b - \frac{1}{z_1 - z_2}\ln\frac{-z_2c_2^b}{z_1c_1^b},\\
c_1^{a,l} =& \frac{1}{z_1}(z_1c_1^a)^{\frac{-z_2}{z_1-z_2}}(-z_2c_2^a)^{\frac{z_1}{z_1-z_2}}, \quad c_2^{a,l} = -\frac{1}{z_2}(z_1c_1^a)^{\frac{-z_2}{z_1-z_2}}(-z_2c_2^a)^{\frac{z_1}{z_1-z_2}},\\
c_1^{b,r} =& \frac{1}{z_1}(z_1c_1^b)^{\frac{-z_2}{z_1-z_2}}(-z_2c_2^b)^{\frac{z_1}{z_1-z_2}}, \quad c_2^{b,r} = -\frac{1}{z_2}(z_1c_1^b)^{\frac{-z_2}{z_1-z_2}}(-z_2c_2^b)^{\frac{z_1}{z_1-z_2}},\\
c_1^{a,m} =& e^{z_1(\phi^a - \phi^{a,m})}c_1^a, \quad c_1^{b,m} = e^{z_1(\phi^b - \phi^{b,m})}c_1^b,\\
H(x) =& \int_0^x \frac{1}{h(s)}ds.
\end{aligned} \tag{2.11}$$

Remark 2.2. *In (2.10), the unknowns are:* ϕ^a, ϕ^b, c_1^a, c_2^a, c_1^b, c_2^b, J_1, $\phi^{a,m}$, $\phi^{b,m}$, y^*, *and* Q_0, *that is, there are eleven unknowns that match the total number of equations on (2.10).*

Remark 2.3. *In the upcoming sections, we will encounter lengthy terms in certain formulas. To simplify our notation, we introduce the following abbreviations for* $k = 0, 1, 2$*:*

$$I_k = z_1J_{1k} + z_2J_{2k}, \quad T_k = J_{1k} + J_{2k}. \tag{2.12}$$

3. Expanding singular solutions in the presence of small permanent charge

This section, and particularly Section 3.2, involves numerous intricate computations, undertaken with rigorous precision and validated through multiple verifications. However, to maintain readability, the detailed computations have been presented in compact form within the text. Interested readers are encouraged to meticulously examine each step and process to replicate the results accurately. Detailed computations pertaining to Section 3.1 can be found in the papers [16, 17]. Additionally, for further clarification on Section 3.2, the authors are available upon request and can provide a comprehensive version of the paper to the journal if necessary.

Assuming that $|Q_0|$ is small, we expand all unknown quantities in the governing system (2.10) and (2.11) in Q_0, i.e., we write

$$\begin{aligned}
&\phi^a = \phi_0^a + \phi_1^aQ_0 + \phi_2^aQ_0^2 + O(Q_0^3), \quad \phi^b = \phi_0^b + \phi_1^bQ_0 + \phi_2^bQ_0^2 + O(Q_0^3),\\
&c_k^a = c_{k0}^a + c_{k1}^aQ_0 + c_{k2}^aQ_0^2 + O(Q_0^3), \quad c_k^b = c_{k0}^b + c_{k1}^bQ_0 + c_{k2}^bQ_0^2 + O(Q_0^3),\\
&y = y_0 + y_1Q_0 + y_2Q_0^2 + O(Q_0^3), \quad J_k = J_{k0} + J_{k1}Q_0 + J_{k2}Q_0^2 + O(Q_0^3),\\
&I = I_0 + I_1Q_0 + I_2Q_0^2 + O(Q_0^3),
\end{aligned} \tag{3.1}$$

where, I_k, for $k = 0, 1, 2$, were defined in (2.12).

Remark 3.1. *To simplify matters, we made the assumption that all diffusion coefficients* D_k *in (2.3) are equal. Therefore, we did not include them in our calculations in (3.1).*

Remark 3.2. *In the upcoming sections, as illustrated in (3.1), the subscripts 's' in* $\phi_s^a, c_{ks}^a, J_{ks}$, *etc., indicate the term's order when expanded with respect to* Q_0. *Here, 's' can represent values of* $0, 1$, *or* 2, *corresponding to the zeroth, first, or second-order term, respectively.*

3.1. Zeroth and first order solutions in Q_0 of (2.10) and (2.11).

The problem for the limiting case, where $Q_0 = 0$, has been addressed in [17] for $h(x) = 1$, and for a general $h(x)$, it can be resolved as demonstrated in [14] over the interval $[0, a]$. One can also derive the zeroth order solution directly by substituting Eq (3.1) into (2.10), expanding the identities in Q_0, and comparing the terms of like-powers in Q_0. Below, we outline the results for the zeroth and first order terms. The detailed proofs for these solutions can be referenced in [16]. These expressions are essential for the computational calculations discussed in Section 4.1, as well as for the computations related to second-order solutions in Section 4.2. Denote,

$$\alpha = \frac{H(a)}{H(1)} \quad \text{and} \quad \beta = \frac{H(b)}{H(1)}, \tag{3.2}$$

where $H(x)$ was defined in (2.11). Note that if $h(x)$ is uniform, then $H(x)$ represents the ratio of the length to the cross-sectional area of the portion of the channel over the interval from 0 to x [35]. The origin of this quantity, $H(x)$, can be traced back to Ohm's law for the resistance of a uniform resistor. It is important to highlight that the parameters a and b, along with the value Q_0, play pivotal roles in defining the shape and the permanent charge of the channel structure. For a more comprehensive understanding of the influences of a and b on the fluxes, refer to Section 4 in [16].

Proposition 3.1. *The zeroth order solutions in Q_0 of (2.10) and (2.11), under electroneutrality boundary conditions $z_1L_1 = -z_2L_2 = L$ and $z_1R_1 = -z_2R_2 = R$ where one obtains $c_j^L = L_j, c_j^R = R_j, \phi^L = V, \phi^R = 0$, are given by*

$$\begin{aligned}
&z_1c_{10}^{a,l} = z_1c_{10}^{a,m} = z_1c_{10}^{a} = (1-\alpha)L + \alpha R, \quad z_1c_{10}^{a} = -z_2c_{20}^{a},\\
&z_1c_{10}^{b,m} = z_1c_{10}^{b,r} = z_1c_{10}^{b} = (1-\beta)L + \beta R, \quad z_1c_{10}^{b} = -z_2c_{20}^{b},\\
&\phi_0^{a,l} = \phi_0^{a,m} = \phi_0^{a} = \frac{\ln\left((1-\alpha)L + \alpha R\right) - \ln R}{\ln L - \ln R}V,\\
&\phi_0^{b,m} = \phi_0^{b,r} = \phi_0^{b} = \frac{\ln\left((1-\beta)L + \beta R\right) - \ln R}{\ln L - \ln R}V,\\
&y_0 = \frac{H(1)}{(z_1 - z_2)(L-R)} \ln \frac{(1-\alpha)L + \alpha R}{(1-\beta)L + \beta R},\\
&J_{10} = \frac{L-R}{z_1H(1)(\ln L - \ln R)}(z_1V + \ln L - \ln R),\\
&J_{20} = -\frac{L-R}{z_2H(1)(\ln L - \ln R)}(z_2V + \ln L - \ln R).
\end{aligned}$$

To compute the first-order terms in Q_0, we adopt the method introduced in [16], where we represent the intermediate variables in relation to the zeroth-order terms. The proof process is straightforward: by expanding the relevant identities in (2.11) with respect to Q_0, comparing the first-order terms in Q_0, and utilizing the results derived from Proposition (3.1), we can establish the desired relations.

Lemma 3.2. *For the first order solution in Q_0 of (2.10) and (2.11), we obtain*

$$
\begin{aligned}
&z_1c_{11}^a + z_2c_{21}^a = -\frac{1}{2}, \qquad \phi_1^{a,m} = \phi_1^a + \frac{1}{2z_1(z_1-z_2)c_{10}^a},\\
&z_1c_{11}^b + z_2c_{21}^b = -\frac{1}{2}, \qquad \phi_1^{b,m} = \phi_1^b + \frac{1}{2z_1(z_1-z_2)c_{10}^b},\\
&\phi_1^{a,l} = \phi_1^a - \frac{c_{10}^a c_{21}^a - c_{20}^a c_{11}^a}{(z_1-z_2)c_{10}^a c_{20}^a}, \quad c_{11}^{a,l} = \frac{z_2(c_{11}^a + c_{21}^a)}{z_2 - z_1}, \quad c_{21}^{a,l} = \frac{z_1(c_{11}^a + c_{21}^a)}{z_1 - z_2},\\
&c_{11}^{a,m} = c_{11}^a - \frac{1}{2(z_1-z_2)}, \quad c_{11}^{b,m} = c_{11}^b - \frac{1}{2(z_1-z_2)},\\
&\phi_1^{b,r} = \phi_1^b - \frac{c_{10}^b c_{21}^b - c_{20}^b c_{11}^b}{(z_1-z_2)c_{10}^b c_{20}^b}, \quad c_{11}^{b,r} = \frac{z_2(c_{11}^b + c_{21}^b)}{z_2 - z_1}, \quad c_{21}^{b,r} = \frac{z_1(c_{11}^b + c_{21}^b)}{z_1 - z_2}.
\end{aligned}
$$

By applying the same procedure as above to the remaining four identities in (2.10), and utilizing the results from Proposition (3.1) and Lemma (3.2), one can directly derive the first-order terms as follows.

Proposition 3.3. *The first-order terms of the solution in Q_0 for the system (2.10) are as follows:*

$$
\begin{aligned}
c_{11}^a &= \frac{z_2\alpha(\phi_0^b - \phi_0^a)}{z_1 - z_2} - \frac{1}{2(z_1-z_2)}, \qquad c_{21}^a = \frac{z_1\alpha(\phi_0^b - \phi_0^a)}{z_2 - z_1} - \frac{1}{2(z_2-z_1)},\\
c_{11}^b &= \frac{z_2(1-\beta)(\phi_0^a - \phi_0^b)}{z_1 - z_2} - \frac{1}{2(z_1-z_2)}, \quad c_{21}^b = \frac{z_1(1-\beta)(\phi_0^a - \phi_0^b)}{z_2 - z_1} - \frac{1}{2(z_2-z_1)},\\
\phi_1^a &= \frac{(1+z_1\lambda)(1+z_2\lambda)(c_{10}^b - c_{10}^a)(\ln c_1^L - \ln c_{10}^a)}{z_1(z_1-z_2)c_{10}^a c_{10}^b(\ln c_1^R - \ln c_1^L)} + \frac{1}{2z_1(z_1-z_2)c_{10}^a} + \frac{z_2\alpha(\phi_0^b - \phi_0^a)}{(z_1-z_2)c_{10}^a}\lambda,\\
\phi_1^b &= \frac{(1+z_1\lambda)(1+z_2\lambda)(c_{10}^b - c_{10}^a)(\ln c_1^R - \ln c_{10}^b)}{z_1(z_1-z_2)c_{10}^a c_{10}^b(\ln c_1^R - \ln c_1^L)} + \frac{1}{2z_1(z_1-z_2)c_{10}^b} + \frac{z_2(1-\beta)(\phi_0^a - \phi_0^b)}{(z_1-z_2)c_{10}^b}\lambda,\\
y_1 &= \frac{\Big((1-\beta)c_1^L + \alpha c_1^R\Big)(\phi_0^a - \phi_0^b)}{z_1(z_1-z_2)T_0 c_{10}^a c_{10}^b} + \frac{(\ln c_{10}^a - \ln c_{10}^b)(\phi_0^a - \phi_0^b)}{z_1(z_1-z_2)T_0(c_1^L - c_1^R)} - \frac{(z_2J_{10} + z_1J_{20})(c_{10}^a - c_{10}^b)}{z_1^2 z_2(z_1-z_2)T_0^2 c_{10}^a c_{10}^b},\\
J_{11} &= \frac{A\Big(z_2(1-B)V + \ln L - \ln R\Big)}{(z_1-z_2)H(1)(\ln L - \ln R)^2}(z_1V + \ln L - \ln R),\\
J_{21} &= \frac{A\Big(z_1(1-B)V + \ln L - \ln R\Big)}{(z_2-z_1)H(1)(\ln L - \ln R)^2}(z_2V + \ln L - \ln R),
\end{aligned}
$$

where, under electroneutrality boundary conditions $z_1L_1 = -z_2L_2 = L$ and $z_1R_1 = -z_2R_2 = R$, and in terms of $\alpha = \frac{H(a)}{H(1)}$ and $\beta = \frac{H(b)}{H(1)}$, the expressions for A, B and λ are

$$
\begin{aligned}
A &= A(L,R) = -\frac{(\beta-\alpha)(L-R)^2}{\Big((1-\alpha)L + \alpha R\Big)\Big((1-\beta)L + \beta R\Big)(\ln L - \ln R)},\\
B &= B(L,R) = \frac{1}{A}\ln\frac{(1-\beta)L + \beta R}{(1-\alpha)L + \alpha R}, \qquad \lambda = \lambda(L,R) = \frac{V}{\ln L - \ln R}.
\end{aligned}
\tag{3.3}
$$

3.2. Second order solutions in Q_0 of (2.10) and (2.11).

The results presented in this section extend the findings of the previous section, employing a consistent approach and methodologies with solutions exhibiting regularity concerning the permanent charge. To date, as far as we know, other papers have examined only up to the first-order terms in Eq (3.1), and the quadratic expression obtained in Section 3.2 is introduced for the first time in this work. Hence, all results in this section represent novel findings. Nevertheless, it is crucial to note that certain intricate calculations, owing to their extensive nature, are condensed for the sake of clarity in the presentation. For the second order solutions in terms of Q_0, we will first express the intermediate variables such as $\phi_2^{a,l}$, $c_{k2}^{a,l}$, etc. in terms of zeroth and first order terms and ϕ_2^a, c_{k2}^a, etc.

Lemma 3.4. *For the second-order solutions in terms of Q_0, we have*

$$z_1c_{12}^a + z_2c_{22}^a = -\frac{z_1+z_2}{24z_1(z_1-z_2)c_{10}^a}, \quad \phi_2^a - \phi_2^{a,m} = \frac{z_1^2c_{11}^a + z_2^2c_{21}^a}{2(z_1(z_1-z_2)c_{10}^a)^2} - \frac{z_1+z_2}{12(z_1(z_1-z_2)c_{10}^a)^2},$$
$$z_1c_{12}^b + z_2c_{22}^b = -\frac{z_1+z_2}{24z_1(z_1-z_2)c_{10}^b}, \quad \phi_2^b - \phi_2^{b,m} = \frac{z_1^2c_{11}^b + z_2^2c_{21}^b}{2(z_1(z_1-z_2)c_{10}^b)^2} - \frac{z_1+z_2}{12(z_1(z_1-z_2)c_{10}^b)^2}.$$

Proof. We present the derivations of the first two equations without showing the tedious computations, which mainly involve manipulating lengthy terms. The first step is to substitute (3.1) into the first equation in (2.10) and expand with respect to the parameter Q_0. Then, by applying a Taylor expansion for the function $e^{z_k(\phi^a-\phi^{a,m})}$ with respect to Q_0, we obtain the following expression for the second order terms:

$$\phi_2^a - \phi_2^{a,m} = -\frac{z_1c_{12}^a + z_2c_{22}^a}{z_1(z_1-z_2)c_{10}^a} + \frac{z_1^2c_{11}^a + z_2^2c_{21}^a}{2(z_1(z_1-z_2)c_{10}^a)^2} - \frac{z_1^3c_{10}^a + z_2^3c_{20}^a}{8(z_1(z_1-z_2)c_{10}^a)^3}. \tag{3.4}$$

Next, we substitute the expression for $c_1^{a,l}$ from $c_1^{a,l}$ from (2.11) into the third equation of (2.10) and expand the resulting equation up to third-order terms in Q_0, which gives us:

$$\frac{z_2-z_1}{z_2}\Big(\frac{1}{z_1}(z_1c_1^a)^{\frac{-z_2}{z_1-z_2}}(-z_2c_2^a)^{\frac{z_1}{z_1-z_2}}\Big) = c_1^ae^{z_1(\phi^a-\phi^{a,m})} + c_2^ae^{z_2(\phi^a-\phi^{a,m})} + Q_0(\phi^a - \phi^{a,m}). \tag{3.5}$$

To obtain the desired result, we must carefully compute the expansions on both sides of (3.5) up to the third order and simplify the terms accordingly. to obtain the desired result.

Note that for small values of Q_0, we can make an approximation: $z_1c_1^a + z_2c_2^a \approx z_1c_{10}^a + z_2c_{20}^a = 0$, which implies that $-z_2c_2^a/z_1c_1^a \approx 1$. Moreover, in the proof, we applied the Maclaurin expansion of the natural logarithm, given by $\ln(x) = \ln(1+(x-1)) = (x-1) - \frac{1}{2}(x-1)^2 + \cdots$. This expansion converges when $|x-1| < 1$.

Lemma 3.5. *For the second-order intermediate variables in terms of Q_0, we establish*

$$\phi_2^{a,l} = \phi_2^a + \frac{z_1 z_2 \alpha(\phi_0^b - \phi_0^a)}{2\left(z_1(z_1 - z_2)c_{10}^a\right)^2} - \frac{z_1 + z_2}{6\left(z_1(z_1 - z_2)c_{10}^a\right)^2}, \quad c_{12}^{a,l} = \frac{z_2(c_{12}^a + c_{22}^a)}{z_2 - z_1} + \frac{z_2}{8z_1 c_{10}^a (z_1 - z_2)^2},$$
$$\phi_2^{b,r} = \phi_2^b + \frac{z_1 z_2 (1-\beta)(\phi_0^a - \phi_0^b)}{2\left(z_1(z_1 - z_2)c_{10}^b\right)^2} - \frac{z_1 + z_2}{6\left(z_1(z_1 - z_2)c_{10}^b\right)^2}, \quad c_{12}^{b,r} = \frac{z_2(c_{12}^b + c_{22}^b)}{z_2 - z_1} + \frac{z_2}{8z_1 c_{10}^b (z_1 - z_2)^2},$$
$$c_{22}^{a,l} = \frac{z_1(c_{12}^a + c_{22}^a)}{z_1 - z_2} - \frac{z_1}{8z_1 c_{10}^a (z_1 - z_2)^2}, \qquad c_{22}^{b,r} = \frac{z_1(c_{12}^b + c_{22}^b)}{z_1 - z_2} - \frac{z_1}{8z_1 c_{10}^b (z_1 - z_2)^2}$$
$$c_{12}^{a,m} = c_{12}^a + \frac{z_1 - 8z_2}{24 z_1 (z_1 - z_2)^2 c_{10}^a}, \qquad c_{12}^{b,m} = c_{12}^b + \frac{z_1 - 8z_2}{24 z_1 (z_1 - z_2)^2 c_{10}^b}.$$

Proof. Starting from the second line of (2.11), we can derive the second order terms as follows:

$$\phi_2^{a,l} = \phi_2^a + \frac{12 z_1(z_1 - z_2)c_{11}^a + 2(z_1 - 2z_2)}{24\left(z_1(z_1 - z_2)c_{10}^a\right)^2}.$$

By substituting c_{11}^a from Proposition (3.3), we obtain the formula for $\phi_2^{a,l}$.

Moving on to the fourth line of (2.11), the second order terms can be expressed as:

$$c_{12}^{a,l} = \frac{z_2(c_{12}^a + c_{22}^a)}{z_2 - z_1} + \frac{z_2}{8z_1 c_{10}^a (z_1 - z_2)^2}.$$

Finally, from the sixth line of (2.11), we can determine $c_{12}^{a,m}$. Similar relations can be found for the other terms.

By following the previously outlined procedure for the last four identities in (2.10) and leveraging the results from Proposition (3.3), along with Lemmas (3.4) and (3.5), one can straightforwardly derive the following Lemma.

Lemma 3.6. *Second order fluxes of the solution in Q_0 to the system 2.10 are given by*

$$\begin{aligned}
J_{12} =& \frac{z_2(c_{12}^a + c_{22}^a)}{(z_1 - z_2)\alpha H(1)}\left(1 + \frac{z_1(\phi^L - \phi_0^a)}{\ln c_1^L - \ln c_{10}^a} - \frac{z_1(\phi^L - \phi_0^a)(c_1^L - c_{10}^a)}{(\ln c_1^L - \ln c_{10}^a)^2 c_{10}^a}\right) \\
&- \frac{z_1(c_1^L - c_{10}^a)}{\alpha H(1)(\ln c_1^L - \ln c_{10}^a)}\Bigg(\phi_2^a + \frac{z_1 z_2 \alpha(\phi_0^b - \phi_0^a)}{2\left(z_1(z_1 - z_2)c_{10}^a\right)^2} - \frac{z_1 + z_2}{6\left(z_1(z_1 - z_2)c_{10}^a\right)^2} \\
&- \frac{z_2(\phi^L - \phi_0^a)}{8z_1(z_1 - z_2)^2(\ln c_1^L - \ln c_{10}^a)(c_{10}^a)^2}\Bigg) \\
&- \frac{z_1 z_2(c_{11}^a + c_{21}^a)}{\alpha H(1)(\ln c_1^L - \ln c_{10}^a)(z_1 - z_2)}\Bigg(\phi_1^a - \frac{(c_1^L - c_{10}^a)\phi_1^a}{(\ln c_1^L - \ln c_{10}^a)c_{10}^a} - \frac{1}{2z_1(z_1 - z_2)c_{10}^a} \\
&+ \frac{c_1^L - c_{10}^a}{2z_1(z_1 - z_2)(\ln c_1^L - \ln c_{10}^a)(c_{10}^a)^2} + \frac{z_2(c_{11}^a + c_{21}^a)(\phi^L - \phi_0^a)(c_1^L + c_{10}^a)}{2(z_1 - z_2)(\ln c_1^L - \ln c_{10}^a)(c_{10}^a)^2}\Bigg) \\
&- \frac{z_1 z_2(\phi^L - \phi_0^a)}{8z_1(z_1 - z_2)^2 c_{10}^a \alpha H(1)(\ln c_1^L - \ln c_{10}^a)} - \frac{z_2}{8z_1 c_{10}^a (z_1 - z_2)^2 \alpha H(1)},
\end{aligned}$$

$$
\begin{aligned}
J_{22} =& -\frac{z_1(c_{12}^a + c_{22}^a)}{(z_1 - z_2)\alpha H(1)}\Big(1 + \frac{z_2(\phi^L - \phi_0^a)}{\ln c_2^L - \ln c_{20}^a} - \frac{z_2(\phi^L - \phi_0^a)(c_2^L - c_{20}^a)}{(\ln c_2^L - \ln c_{20}^a)^2 c_{20}^a}\Big) \\
& - \frac{z_2(c_2^L - c_{20}^a)}{\alpha H(1)(\ln c_2^L - \ln c_{20}^a)}\Bigg(\phi_2^a + \frac{z_1 z_2 \alpha(\phi_0^b - \phi_0^a)}{2\big(z_1(z_1 - z_2)c_{10}^a\big)^2} - \frac{z_1 + z_2}{6\big(z_1(z_1 - z_2)c_{10}^a\big)^2} \\
& + \frac{z_1(\phi^L - \phi_0^a)}{8z_1(z_1 - z_2)^2(\ln c_2^L - \ln c_{20}^a)c_{10}^a c_{20}^a}\Bigg) \\
& + \frac{z_1 z_2(c_{11}^a + c_{21}^a)}{\alpha H(1)(\ln c_2^L - \ln c_{20}^a)(z_1 - z_2)}\Big(\phi_1^a - \frac{(c_2^L - c_{20}^a)\phi_1^a}{(\ln c_2^L - \ln c_{20}^a)c_{20}^a} - \frac{1}{2z_1(z_1 - z_2)c_{10}^a} \\
& + \frac{c_2^L - c_{20}^a}{2z_1(z_1 - z_2)(\ln c_2^L - \ln c_{20}^a)(c_{10}^a)(c_{20}^a)} - \frac{z_1(c_{11}^a + c_{21}^a)(\phi^L - \phi_0^a)(c_2^L + c_{20}^a)}{2(z_1 - z_2)(\ln c_2^L - \ln c_{20}^a)(c_{20}^a)^2}\Big) \\
& + \frac{z_1 z_2(\phi^L - \phi_0^a)}{8z_1(z_1 - z_2)^2 c_{10}^a \alpha H(1)(\ln c_2^L - \ln c_{20}^a)} + \frac{z_1}{8z_1 c_{10}^a(z_1 - z_2)^2 \alpha H(1)},
\end{aligned}
$$

where,

$$
K_1 = T_0 y_1 + T_1 y_0, \quad K_2 = T_2 y_0 + T_1 y_1 + T_0 y_2,
$$

and T_0, T_1 and T_2 were defined in (2.12).

Proof. Consider the expression J_1 in (2.10), and expand the terms with respect to Q_0 to get,

$$
\begin{aligned}
\frac{c_1^L - c_1^{a,l}}{H(a)} =& \frac{c_1^L - c_{10}^a - c_{11}^{a,l}Q_0 - c_{12}^{a,l}Q_0^2}{\alpha H(1)}, \\
\frac{(c_1^L - c_1^{a,l})}{H(a)}\frac{z_1(\phi^L - \phi^{a,l})}{\ln c_1^L - \ln c_1^{a,l}} =& \Big(c_1^L - c_{10}^a - c_{11}^{a,l}Q_0 - c_{12}^{a,l}Q_0^2\Big) \cdot \Big(\phi^L - \phi_0^a - \phi_1^{a,l}Q_0 - \phi_2^{a,l}Q_0^2\Big) \\
& \cdot \frac{z_1\big(\ln c_1^L - \ln c_{10}^a + \frac{c_{11}^{a,l}}{c_{10}^a}Q_0 + \frac{2c_{12}^{a,l}c_{10}^a - (c_{11}^{a,l})^2}{2(c_{10}^a)^2}Q_0^2\big)}{\alpha H(1)(\ln c_1^L - \ln c_{10}^a)^2}.
\end{aligned}
$$

Therefore, the zeroth and first order terms in Q_0 of J_1 are,

$$
\begin{aligned}
J_{10} =& \frac{c_1^L - c_{10}^a}{\alpha H(1)} + \frac{z_1(c_1^L - c_{10}^a)(\phi^L - \phi_0^a)}{\alpha H(1)(\ln c_1^L - \ln c_{10}^a)}, \\
J_{11} =& -\frac{z_1(c_1^L - c_{10}^a)}{\alpha H(1)(\ln c_1^L - \ln c_{10}^a)}\Bigg(\phi_1^{a,l} - \frac{c_{11}^{a,l}(\phi^L - \phi_0^a)}{(\ln c_1^L - \ln c_{10}^a)c_{10}^a}\Bigg) \\
& - \frac{z_2(c_{11}^a + c_{21}^a)}{(z_2 - z_1)\alpha H(1)} - \frac{z_1 c_{11}^a(\phi^L - \phi_0^a)}{\alpha H(1)(\ln c_1^L - \ln c_{10}^a)}.
\end{aligned}
$$

The second-order term in Q_0 of J_1, with a careful computation, will be as follows,

$$\begin{aligned}
J_{12} =&\frac{z_2(c_{12}^a + c_{22}^a)}{(z_1 - z_2)\alpha H(1)} - \frac{z_2}{8z_1c_{10}^a(z_1 - z_2)^2\alpha H(1)}\\
&- \frac{z_1(c_1^L - c_{10}^a)}{\alpha H(1)(\ln c_1^L - \ln c_{10}^a)}\Big(\phi_2^a + \frac{z_1z_2\alpha(\phi_0^b - \phi_0^a)}{2(z_1(z_1 - z_2)c_{10}^a)^2} - \frac{z_1 + z_2}{6(z_1(z_1 - z_2)c_{10}^a)^2}\Big)\\
&+ \frac{z_1c_{11}^{a,l}\phi_1^{a,l}}{\alpha H(1)(\ln c_1^L - \ln c_{10}^a)}\Big(1 - \frac{c_1^L - c_{10}^a}{(\ln c_1^L - \ln c_{10}^a)c_{10}^a}\Big)\\
&- \frac{z_1c_{12}^{a,l}(\phi^L - \phi_0^a)}{\alpha H(1)(\ln c_1^L - \ln c_{10}^a)}\Big(1 - \frac{(c_1^L - c_{10}^a)}{(\ln c_1^L - \ln c_{10}^a)c_{10}^a}\Big)\\
&- \frac{z_1(c_{11}^{a,l})^2(\phi^L - \phi_0^a)}{\alpha H(1)(\ln c_1^L - \ln c_{10}^a)^2c_{10}^a}\Big(1 + \frac{c_1^L - c_{10}^a}{2c_{10}^a}\Big).
\end{aligned}$$

By substituting $c_{11}^{a,l}$, $c_{12}^{a,l}$, and $\phi_1^{a,l}$ as per Lemmas 3.2 and 3.5, we can directly derive the formula for J_{12}. The expression for J_{22} can be obtained in a similar manner.

Proposition 3.7. *Second order intermediate concentration terms of the solution in Q_0 to the system 2.10 are given by*

$$\begin{aligned}
c_{12}^a =&- \frac{z_1 + 4z_2}{24z_1(z_1 - z_2)^2c_{10}^a} - \frac{(\phi_1^a - \phi_1^b)\alpha z_2}{(z_1 - z_2)},\\
c_{22}^a =&\frac{4z_1 + z_2}{24z_1(z_1 - z_2)^2c_{10}^a} + \frac{(\phi_1^a - \phi_1^b)\alpha z_1}{(z_1 - z_2)},\\
c_{12}^b =&- \frac{z_1 + 4z_2}{24z_1(z_1 - z_2)^2c_{10}^b} + \frac{(\phi_1^a - \phi_1^b)(1 - \beta)z_2}{(z_1 - z_2)},\\
c_{22}^b =&\frac{4z_1 + z_2}{24z_1(z_1 - z_2)^2c_{10}^b} - \frac{(\phi_1^a - \phi_1^b)(1 - \beta)z_1}{(z_1 - z_2)},\\
y_2 =&\frac{(\phi_1^a - \phi_1^b)y_0}{H(1)T_0} - \frac{y_1}{c_{10}^a}\Big(\frac{z_2\alpha(\phi_0^b - \phi_0^a)}{z_1 - z_2} - \frac{c_{10}^a(\phi_0^a - \phi_0^b)}{H(1)T_0} - \frac{1}{z_1 - z_2}\Big)\\
&+ \frac{1}{2z_1^2(z_1 - z_2)^2T_0}\Big(\frac{1}{(c_{10}^a)^2} - \frac{1}{(c_{10}^b)^2}\Big) + \frac{(\phi_1^a - \phi_1^b)}{z_1(z_1 - z_2)T_0}\Big(\frac{\alpha}{c_{10}^a} + \frac{1 - \beta}{c_{10}^b}\Big)\\
&- \frac{z_1z_2}{2T_0}\Big(T_0y_1 + T_1y_0\Big)^2 + \frac{(\phi_0^a - \phi_0^b)y_0}{H(1)T_0c_{10}^a}\Big(\frac{z_2\alpha(\phi_0^b - \phi_0^a)}{z_1 - z_2} - \frac{1}{z_1 - z_2}\Big)\\
&+ \frac{J_{11}}{z_1^2z_2T_0^2}\Big(\frac{1}{c_{10}^b} - \frac{1}{c_{10}^a}\Big) + \frac{J_{10}(\phi_0^a - \phi_0^b)}{z_1^2z_2T_0^3H(1)}\Big(\frac{1}{c_{10}^b} - \frac{1}{c_{10}^a}\Big).
\end{aligned}$$

Proof. Initially, we start by adding up the expressions for J_{12} and J_{22} as outlined in the equations for J_{12} and J_{22} in Lemma 3.6, using careful simplification procedures. Afterward, we include c_{22}^a and c_{22}^b into the derived expression using the relevant expressions from Lemma 3.4. Through comprehensive computational analysis, we determine the expressions for c_{12}^a and c_{22}^a.

In the process of determining the variable y_2, our initial step involves solving the equation for c_{12}^b as presented in Lemma 3.6, specifically for K_2. Following this, we proceed to substitute the expressions for K_1 and K_2 and subsequently solve the equation for y_2, resulting in a simplified expression that provides the formula for y_2.

Remark 3.3. *It is important to mention that because there are no explicit solutions for ϕ_2^a at this stage, the fluxes J_{12} and J_{22} in Lemma 3.6 cannot be expressed explicitly. Therefore, additional simplifications are required to compute the expression for ϕ_2^a, as demonstrated in Proposition 3.8.*

Utilizing the procedure outlined earlier, we shall extend our analysis to encompass the remaining four identities specified in Eq (2.10). With the foundational insights obtained from Proposition (3.1) and Lemma (3.2), we can proceed to systematically deduce the second order terms as delineated below.

Proposition 3.8. *Under the electroneutrality boundary conditions, where $\phi^L = V, \phi^R = 0$, $z_l L_1 = -z_2 L_2 = L$ and $z_l R_1 = -z_2 R_2 = R$, the following results hold,*

$$\begin{aligned}
J_{12} = {} & \frac{z_1 z_2(\phi_1^a - \phi_1^b)}{H(1)(z_1 - z_2)}\Big(\frac{1}{z_1} + \frac{(V - \phi_0^a)}{\ln c_1^L - \ln c_{10}^a} - \frac{(V - \phi_0^a)(c_1^L - c_{10}^a)}{(\ln c_1^L - \ln c_{10}^a)^2 c_{10}^a}\Big) \\
& - \frac{z_1(c_1^L - c_{10}^a)}{\alpha H(1)(\ln c_1^L - \ln c_{10}^a)}\Big(\phi_2^a + \frac{z_1 z_2 \alpha(\phi_0^b - \phi_0^a)}{2\big(z_1(z_1 - z_2)c_{10}^a\big)^2} - \frac{(z_1 + z_2)}{6\big(z_1(z_1 - z_2)c_{10}^a\big)^2}\Big) \\
& - \frac{z_1 z_2(\phi_0^a - \phi_0^b)}{H(1)(\ln c_1^L - \ln c_{10}^a)(z_1 - z_2)^2}\Bigg((z_1 - z_2)\phi_1^a - \frac{(z_1 - z_2)(c_1^L - c_{10}^a)\phi_1^a}{(\ln c_1^L - \ln c_{10}^a)c_{10}^a} - \frac{1}{2z_1 c_{10}^a} \\
& \qquad + \frac{(c_1^L - c_{10}^a)}{2z_1(\ln c_1^L - \ln c_{10}^a)(c_{10}^a)^2} + \frac{z_2(c_{11}^a + c_{21}^a)(V - \phi_0^a)(c_1^L + c_{10}^a)}{2(\ln c_1^L - \ln c_{10}^a)(c_{10}^a)^2}\Bigg),
\end{aligned}$$

$$\begin{aligned}
J_{22} = {} & \frac{z_1 z_2(\phi_1^a - \phi_1^b)}{H(1)(z_2 - z_1)}\Big(\frac{1}{z_2} + \frac{(V - \phi_0^a)}{\ln c_1^L - \ln c_{10}^a} - \frac{(V - \phi_0^a)(c_1^L - c_{10}^a)}{(\ln c_1^L - \ln c_{10}^a)^2 c_{10}^a}\Big) \\
& + \frac{z_1(c_1^L - c_{10}^a)}{\alpha H(1)(\ln c_1^L - \ln c_{10}^a)}\Big(\phi_2^a + \frac{z_1 z_2 \alpha(\phi_0^b - \phi_0^a)}{2\big(z_1(z_1 - z_2)c_{10}^a\big)^2} - \frac{(z_1 + z_2)}{6\big(z_1(z_1 - z_2)c_{10}^a\big)^2}\Big) \\
& + \frac{z_1 z_2(\phi_0^a - \phi_0^b)}{H(1)(\ln c_1^L - \ln c_{10}^a)(z_1 - z_2)^2}\Bigg((z_1 - z_2)\phi_1^a - \frac{(z_1 - z_2)(c_1^L - c_{10}^a)\phi_1^a}{(\ln c_1^L - \ln c_{10}^a)c_{10}^a} - \frac{1}{2z_1 c_{10}^a} \\
& \qquad + \frac{(c_1^L - c_{10}^a)}{2z_1(\ln c_1^L - \ln c_{10}^a)(c_{10}^a)^2} + \frac{z_2(c_{11}^a + c_{21}^a)(V - \phi_0^a)(c_1^L + c_{10}^a)}{2(\ln c_1^L - \ln c_{10}^a)(c_{10}^a)^2}\Bigg),
\end{aligned}$$

$$\begin{aligned}
\phi_2^a &= (\mathcal{B}_1 C - (z_1 - z_2)y_0\mathcal{B}_1\mathcal{A}_2 - z_2 y_0 \mathcal{B}_1\frac{(\phi_1^b - \phi_1^a)}{H(1)} + \mathcal{B}_2 - \mathcal{A}_2)/(\mathcal{A}_1 - \mathcal{B}_1 + (z_1 - z_2)y_0\mathcal{A}_1 B_1), \\
\phi_2^b &= \big(1 - (z_1 - z_2)y_0\mathcal{A}_1\big)\phi_2^a + C - (z_1 - z_2)y_0\mathcal{A}_2 - z_2 y_0\frac{(\phi_1^b - \phi_1^a)}{H(1)},
\end{aligned}$$

where,

$$
\begin{aligned}
\mathcal{A}_1 &= -\frac{z_1(c_1^L - c_{10}^a)}{\alpha H(1)(\ln c_1^L - \ln c_{10}^a)}, \qquad \mathcal{B}_1 = \frac{z_1(c_{10}^b - c_1^R)}{(1-\beta)H(1)(\ln c_{10}^b - \ln c_1^R)},\\
\mathcal{A}_2 &= \frac{z_1z_2(\phi_1^a - \phi_1^b)}{(z_1 - z_2)H(1)}\Big(\frac{1}{z_1} + \frac{(V - \phi_0^a)}{\ln c_1^L - \ln c_{10}^a} - \frac{(V - \phi_0^a)(c_1^L - c_{10}^a)}{(\ln c_1^L - \ln c_{10}^a)^2 c_{10}^a}\Big)\\
&\quad - \frac{z_1(c_1^L - c_{10}^a)}{\alpha H(1)(\ln c_1^L - \ln c_{10}^a)}\Big(\frac{z_1z_2\alpha(\phi_0^b - \phi_0^a)}{2\big(z_1(z_1 - z_2)c_{10}^a\big)^2} - \frac{(z_1 + z_2)}{6\big(z_1(z_1 - z_2)c_{10}^a\big)^2}\Big)\\
&\quad - \frac{z_1z_2(\phi_0^a - \phi_0^b)}{H(1)(\ln c_1^L - \ln c_{10}^a)(z_1 - z_2)^2}\Bigg((z_1 - z_2)\phi_1^a - \frac{(z_1 - z_2)(c_1^L - c_{10}^a)\phi_1^a}{(\ln c_1^L - \ln c_{10}^a)c_{10}^a} - \frac{1}{2z_1c_{10}^a}\\
&\qquad + \frac{(c_1^L - c_{10}^a)}{2z_1(\ln c_1^L - \ln c_{10}^a)(c_{10}^a)^2} + \frac{z_2(c_{11}^a + c_{21}^a)(V - \phi_0^a)(c_1^L + c_{10}^a)}{2(\ln c_1^L - \ln c_{10}^a)(c_{10}^a)^2}\Bigg),\\
\mathcal{B}_2 &= \frac{z_1z_2(\phi_1^a - \phi_1^b)}{(z_1 - z_2)H(1)}\Big(\frac{1}{z_1} + \frac{\phi_0^b}{\ln c_{10}^b - \ln c_1^R} - \frac{\phi_0^b(c_{10}^b - c_1^R)}{(\ln c_{10}^b - \ln c_1^R)^2 c_{10}^b}\Big)\\
&\quad + \frac{z_1(c_{10}^b - c_1^R)}{(1-\beta)H(1)(\ln c_{10}^b - \ln c_1^R)}\Big(\frac{z_1z_2(1-\beta)(\phi_0^a - \phi_0^b)}{2\big(z_1(z_1 - z_2)c_{10}^b\big)^2} - \frac{(z_1 + z_2)}{6\big(z_1(z_1 - z_2)c_{10}^b\big)^2}\Big)\\
&\quad - \frac{z_1z_2(\phi_0^b - \phi_0^a)}{H(1)(\ln c_{10}^b - \ln c_1^R)(z_1 - z_2)^2}\Bigg((z_1 - z_2)\phi_1^b - \frac{(z_1 - z_2)(c_{10}^b - c_1^R)\phi_1^b}{(\ln c_{10}^b - \ln c_1^R)c_{10}^b} - \frac{1}{2z_1c_{10}^b}\\
&\qquad + \frac{(c_{10}^b - c_1^R)}{2z_1(\ln c_{10}^b - \ln c_1^R)(c_{10}^b)^2} + \frac{z_2(c_{11}^b + c_{21}^b)\phi_0^b(c_1^R + c_{10}^b)}{2(\ln c_{10}^b - \ln c_1^R)(c_{10}^b)^2}\Bigg),
\end{aligned}
$$

and,

$$
\begin{aligned}
C &= -\frac{z_1^2c_{11}^a + z_2^2c_{21}^a}{2\big(z_1(z_1 - z_2)c_{10}^a\big)^2} + \frac{z_1^2c_{11}^b + z_2^2c_{21}^b}{2\big(z_1(z_1 - z_2)c_{10}^b\big)^2} + \frac{(z_1 + z_2)\big((c_{10}^b)^2 - (c_{10}^a)^2\big)}{12\big(z_1(z_1 - z_2)c_{10}^a c_{10}^b\big)^2} - I_1y_1\\
&\quad + \frac{(z_1 - z_2)(L - R)Vy_1}{H(1)(\ln L - \ln R)c_{10}^a}\Big(\frac{z_2\alpha(\phi_0^b - \phi_0^a)}{z_1 - z_2} - \frac{c_{10}^a(\phi_0^a - \phi_0^b)}{H(1)T_0} - \frac{1}{z_1 - z_2}\Big)\\
&\quad + \frac{z_2V}{2z_1(z_1 - z_2)^2(\ln L - \ln R)}\Big(\frac{1}{(c_{10}^a)^2} - \frac{1}{(c_{10}^b)^2}\Big)\\
&\quad + \frac{z_1z_2(\phi_1^a - \phi_1^b)V}{(\ln L - \ln R)}\Big(\frac{1}{z_1(z_1 - z_2)}\Big(\frac{\alpha}{c_{10}^a} + \frac{1-\beta}{c_{10}^b}\Big) + \frac{y_0}{H(1)}\Big)\\
&\quad - \frac{z_1^2z_2^2V}{2(\ln L - \ln R)}(T_0y_1 + T_1y_0)^2 + \frac{z_1z_2V(\phi_0^a - \phi_0^b)y_0}{H(1)c_{10}^a(\ln L - \ln R)}\Big(\frac{z_2\alpha(\phi_0^b - \phi_0^a)}{z_1 - z_2} - \frac{1}{z_1 - z_2}\Big)\\
&\quad + \frac{J_{11}V}{z_1T_0(\ln L - \ln R)}\Big(\frac{1}{c_{10}^b} - \frac{1}{c_{10}^a}\Big) + \frac{J_{10}(\phi_0^a - \phi_0^b)V}{z_1T_0^2H(1)(\ln L - \ln R)}\Big(\frac{1}{c_{10}^b} - \frac{1}{c_{10}^a}\Big).
\end{aligned}
$$

Furthermore, $z_1c_1^L = z_1L_1 = L, z_1c_1^R = z_1R_1 = R$ *due to electroneutrality and* T_0, T_1 *were defined in (2.12).*

Proof. Starting from the expressions for J_{12} and J_{22} derived in Lemma 3.6 and employing the relationships established in Lemma 3.5 and Proposition 3.7, and through meticulous computations, one can directly derive the second order terms for fluxes and electric potentials.

Remark 3.4. *In Proposition (3.8), it is noteworthy that the following relationships hold:*

$$J_{12} = \mathcal{A}_1\phi_2^a + \mathcal{A}_2 = \mathcal{B}_1\phi_2^b + \mathcal{B}_2, \qquad J_{22} = -\mathcal{A}_1\phi_2^a + \mathcal{A}_3 = -\mathcal{B}_1\phi_2^b + \mathcal{B}_3,$$

wherein,

$$\mathcal{A}_3 = -\mathcal{A}_2 + \frac{(\phi_1^b - \phi_1^a)}{H(1)}, \qquad \mathcal{B}_3 = -\mathcal{B}_2 + \frac{(\phi_1^b - \phi_1^a)}{H(1)}.$$

Remark 3.5. *We emphasize once more the complex computations used to derive the second-order solutions in Section 3, although they are condensed for readability. Furthermore, Proposition 3.8 provides us with the necessary explicit expressions for the second-order solutions of the fluxes J_{12} and J_{22}. However, given the complexity of these solutions, deriving additional analytical results to examine their impact on flux behavior would be very challenging. Hence, we turn to numerical investigations for further exploration in Section 4.*

4. Impact of permanent charge and boundary conditions on fluxes and I-V relations

In this section, we investigate how permanent charges and the boundary conditions impact the movement of individual fluxes and the current-voltage (I-V) relations. When the magnitude of Q_0 (a measure of permanent charge) is small, the flux J_k for the k-th type of ion and the current I can be represented as in (3.1). The quantities J_{1k} and J_{2k}, where $k = 0, 1, 2$, capture the primary effects of permanent charges and channel shape on the flow of ions. We will analyze these quantities to understand their impact.

Remark 4.1. *In the subsequent sections of this part, we conduct numerical simulations alongside an analysis of the equations in Section 3. The integration of numerical methods and analytical insights enhances our comprehension of the analytical findings. Specifically, the complexity of the quadratic solutions in Section 3.2 necessitates leveraging numerical observations to gain a deeper understanding of the second order solutions and their impact on the system. In our numerical simulations, we choose simplicity and specificity by setting $a = 1/3$, $b = 2/3$ in (2.6), and $h(x) = 1$. As a result, this yields $\alpha = 1/3$ and $\beta = 2/3$ in (3.2).*

As highlighted in the Introduction section, our numerical methods are implemented using Python in conjunction with the Numpy and Matplotlib libraries. We create heatmaps, if possible, to visualize the signs of fluxes in various figures during our investigations, necessitating the identification of roots within the expressions. To accomplish this, we leverage combinations of Python functions, specifically *np.where* and *np.isclose*, for root finding purposes. Additionally, we also tried utilizing some other functions like the *root* function from the em scipy.optimize module, which is commonly used to solve systems of nonlinear equations. Due to the structured nature of our code, we prioritize the *np.where* and *np.isclose* functions. The *np.isclose* function, with its parameters *rtol* (relative tolerance), *atol* (absolute tolerance), and *equal-nan* (specifying 'Not a Number' (NaN) handling), generates a boolean array indicating element-wise equality within specified tolerances. Similarly, *np.where(condition, [x, y])* selects elements from x or *y* based on a given condition, which proves useful when combined with *np.isclose* to locate indices satisfying the condition [37].

4.1. Exploring first-order effects: Influence of permanent charges on fluxes

We begin by revisiting and simplifying specific findings from [16] and presenting numerical results for the first-order terms. Initially, we articulate Theorem 4.8 in [16], providing numerical insights, and subsequently expand on our findings based on further numerical investigations.

Suppose $B \neq 1$ where B is defined as in (3.3). Let V_q^1 and V_q^2 be defined as follows:

$$
\begin{aligned}
V_q^1 &= V_q^1(L,R) = -\frac{\ln L - \ln R}{z_2(1-B)},\\
V_q^2 &= V_q^2(L,R) = -\frac{\ln L - \ln R}{z_1(1-B)}.
\end{aligned} \tag{4.1}
$$

Then the following cases arise:

(i) if $V_q^1 < 0 < V_q^2$, then, for $V > V_q^1$, a small positive Q_0 decreases $|J_1|$, and for $V < V_q^1$, it enhances $|J_1|$. Similarly, for $V > V_q^2$, a small positive Q_0 decreases $|J_2|$, and for $V < V_q^2$, it strengthens $|J_2|$; more precisely,

- (i1) for $V \in (V_q^1, V_q^2)$, $J_{10}J_{11} < 0$ and $J_{20}J_{21} > 0$;
- (i2) for $V < V_q^1$, $J_{10}J_{11} > 0$ and $J_{20}J_{21} > 0$;
- (i3) for $V > V_q^2$, $J_{10}J_{11} < 0$ and $J_{20}J_{21} < 0$;

(ii) if $V_q^1 > 0 > V_q^2$, then, for $V < V_q^1$, a small positive Q_0 decreases $|J_1|$, and for $V > V_q^1$, it enhances $|J_1|$. Similarly, for $V < V_q^2$, a small positive Q_0 decreases $|J_2|$, and for $V > V_q^2$, it strengthens $|J_2|$; more precisely,

- (ii1) for $V \in (V_q^2, V_q^1)$, $J_{10}J_{11} < 0$ and $J_{20}J_{21} > 0$;
- (ii2) for $V > V_q^1$, $J_{10}J_{11} > 0$ and $J_{20}J_{21} > 0$;
- (ii3) for $V < V_q^2$, $J_{10}J_{11} < 0$ and $J_{20}J_{21} < 0$.

The statements above are presented in a more streamlined form based on Theorem 4.8 in [16], which indicates that either case (i) or (ii) may occur regardless of whether $L < R$ or $L > R$. It is crucial to highlight that the roots V_q^1 and V_q^2 in Eq (4.1) correspond to the roots of $J_{10}J_{11}$ and $J_{20}J_{21}$, respectively. This allows us to examine the effects of including linear terms J_{11} or J_{21}. Now, let us extend the aforementioned findings based on the numerical observations depicted in Figure 2. It is also important to note that, with the simplifying assumptions in Remark 4.1, we have standardized the structure of channel geometry to focus on our primary objective, which is analyzing the relationships between the different orders of solutions in terms of Q_0 and boundary conditions, and their effects on fluxes and the I-V relation.

Now, we present a key observation derived from our numerical investigations, which sheds light on critical values and their impact on flux magnitudes under specific conditions regarding channel geometry. The findings from our analysis, summarized below, reveal significant insights into the behavior of fluxes J_1 and J_2 under varying voltage conditions and boundary concentrations:

Given boundary concentrations L and R, and under certain conditions regarding channel geometry we have:

(i) There exist critical values $V_1^* < 0 < V_2^*$ such that:
  (i1) For $V > V_1^*$, a small positive Q_0 reduces $|J_1|$, and for $V < V_1^*$, it amplifies $|J_1|$.
  (i2) For $V > V_2^*$, a small positive Q_0 decreases $|J_2|$, and for $V < V_2^*$, it strengthens $|J_2|$.

(ii) There exist critical points $V_2^* < 0 < V_1^*$ leading to:
(ii1) For $V < V_1^*$, a small positive Q_0 reduces $|J_1|$, and for $V > V_1^*$, it amplifies $|J_1|$.
(ii2) For $V < V_2^*$, a small positive Q_0 decreases $|J_2|$, and for $V > V_2^*$, it strengthens $|J_2|$.

It is worth nothing that the detailed cases can be articulated similarly to the detailed parts in Theorem 4.8 in [16]. Additionally, it is important to notice that V_1^* and V_2^* denote V_q^1 and V_q^2 respectively, although they are derived from numerical results.

Below is an observation derived from our numerical investigations. While the theoretical proof is not overly challenging, we opt not to consider it. The following findings are noted:

(a) When the boundary concentrations on the left and right (L and R, respectively) are nearly identical ($L \approx R$), a small positive Q_0 decreases $|J_1|$ while increasing $|J_2|$. This behavior is exemplified by the blue region near $L = 1$ in Figure 2(A) and the red region near $L = 1$ in Figure 2(B).

(b) When the boundary concentrations are significantly different, the voltage ranges, for which a small positive Q_0 reduces $|J_1|$, become smaller, as do the voltage ranges for which Q_0 raises $|J_2|$. In other words, as the gap between L and R widens, the blue region in panel (A) and the red region in panel (B) in Figure 2 also reduce. In particular, for a fixed R, let V_1^* and V_2^* represent the critical points of $J_{10}J_{11}$ and $J_{20}J_{21}$ corresponding to L_1 and L_2, respectively, and let $\bar{V}_1^*$ and $\bar{V}_2^*$ denote the critical points of $J_{10}J_{11}$ and $J_{20}J_{21}$ corresponding to $\bar{L}_1$ and $\bar{L}_2$. Refer to Figure 2. This yields:
(b.1) if $R < L_1 < \bar{L}_1$, then $V_1^* < \bar{V}_1^* < 0$ and $0 < \bar{V}_2^* < V_2^*$.
(b.2) if $\bar{L}_1 < L_1 < R$, then $0 < \bar{V}_1^* < V_1^*$ and $V_2^* < \bar{V}_2^* < 0$.

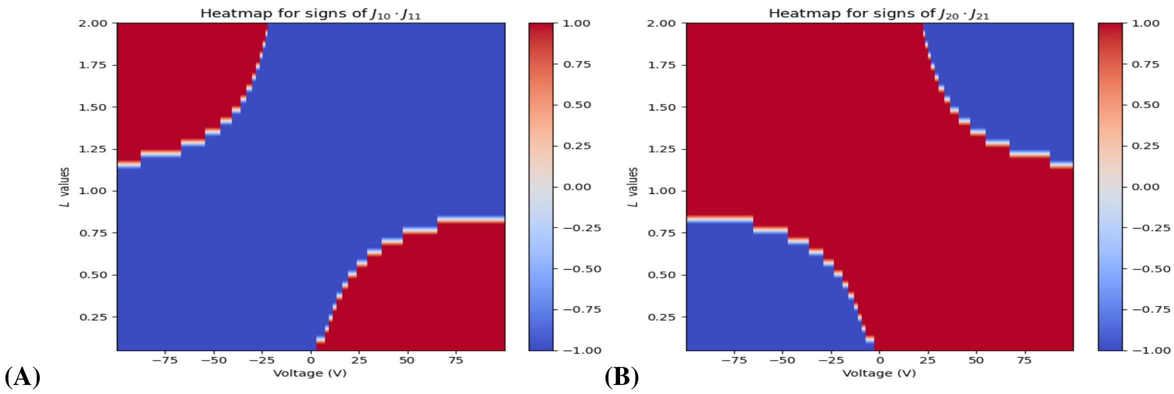

Figure 2. Visualization of heatmaps indicating the sign agreement for the products $J_{10}J_{11}$ (panel A) and $J_{20}J_{21}$ (panel B). The concentration L varies from zero to two while R is fixed at 1, shedding light on the impact of linear terms.

Remark 4.2. *One can check the author's GitHub repository for additional validation of the above observation as well as the upcoming figures in the subsequent sections. Similar situations can also be seen for a fixed L there. The GitHub repository link is: https://github.com/Hamid-Mofidi/PNP/tree/main/Q2contribution.*

Remark 4.3. *In computational plots where it appears that l and r are equal, it is essential to note that they are very close but not precisely equal. This distinction is crucial based on the results.*

The numerical results shown in Figure 2 validate the discussed scenarios, where the right boundary concentration R is fixed at 1, while L is varied between 0 and 2. Initially, this figure presents individual heatmaps illustrating the signs of $J_{10}J_{11}$ and $J_{20}J_{21}$ to clarify their respective flux changes. The red regions indicate areas where J_{10} and J_{11} in panel (A) (or, equivalently, J_{20} and J_{21} in panel (B)) share the same signs, while the blue regions denote areas where the signs are opposite. The color scheme can be interpreted as follows:

a. Red regions indicate areas where a (small) positive Q_0 reinforces $|J_1|$ or $|J_2|$.
b. Blue regions denote areas where a (small) positive Q_0 diminishes $|J_1|$ or $|J_2|$.

Thus far, the validation of our computational approach and analytical findings has been achieved by comparing them with Theorem 4.8 in [16], incorporating both zeroth and first-order terms. Our numerical analyses not only confirmed these findings but also provided additional insights into the first-order terms.

Remark 4.4. *To validate our findings, we employed two approaches in our numerical analysis:*

1) First, we computed V_q^1 and V_q^2 according to Theorem 4.8 *in [16], as outlined at the beginning of this section. We then determined the signs on each interval.*
2) Second, we numerically identified the roots V_1^* and V_2^* without explicitly computing V_q^1 and V_q^2.

We confirmed that the results are consistent for the first-order terms. The latter approach is particularly advantageous when incorporating the second order terms in the subsequent section, as obtaining roots analytically could be challenging. This will be our approach in the following section.

The intricate nature of the second order terms, specifically the fluxes J_{12} and J_{22} discussed in Section 3.2, necessitates numerical approaches to determine their roots. Therefore, we turn to Python, leveraging the Numpy and Matplotlib libraries, to perform calculations for zeroth, first, and the second order terms [37]. Additionally, numerical tools are employed to identify flux roots, facilitating the study of their signs across diverse regions.

The theoretical analysis of complex second order terms in equations provided in Proposition 3.8 is challenging. As a result, we use computational methods to explore how permanent charges affect ion movement and the membrane's electrical behavior, focusing on the current-voltage (I-V) relation. We analyze and compare these outcomes to scenarios without permanent charges, examining how these differences affect membrane performance. Then we study higher order contributions of permanent charges. Our numerical investigation delves into understanding the intricate interactions of permanent charges, shedding light on their influence on crucial electrical properties. Through this exploration, our aim is to advance our comprehension of the system's behavior and offer valuable insights to the academic community.

4.2. Exploring the effects of second-order solutions and boundary conditions on fluxes

As of now, to the best of our knowledge, previous studies have only investigated up to the first-order terms in Eq (3.1) [16], and the quadratic expression obtained in Section 3.2 is introduced for the first time in this work. Incorporating these quadratic terms into the linear solutions will increase the accuracy of the solutions, although it was analytically challenging to derive them.

In this section, we delve into the implications of incorporating the Q_0^2 term into the expressions. Our primary focus is on investigating how the inclusion of J_{k2} influences the linear estimation of J_1, represented as $J_{k0} + J_{k1}Q_0$. Additional comprehensive and noteworthy findings have been uncovered.

Using heatmaps to examine the signs of $(J_{k0} + J_{k1}Q_0)J_{12}$ for $k = 1, 2$, along with the product $J_{k0}J_{k1}J_{k2}$, has revealed deeper insights, highlighting the unique impact of the Q_0^2 terms on the results.

In [15], the author demonstrates that the sign of the flux J_k for $k = 1, 2$ remains unaffected by a permanent charge. In biological and chemical terms, the sign of the flux is dictated by the driving force (the gradient of electrochemical potential) rather than the structure (permanent charge Q_0) of the channel protein. However, the magnitude of J_k is indeed influenced by Q_0. Referring back to 3.1, where for $k = 1, 2$, we have $J_k = J_{k0} + J_{k1}Q_0 + J_{k2}Q_0^2 + O(Q_0^3)$, we now focus on analyzing the impact of J_{k2}, the second order term of the flux, on the magnitude and behavior of J_k using various approaches:

(1) Computing the product $(J_{k0} + J_{k1}Q_0)J_{k2}$ to observe the effects of J_{k2} on the linear estimation of J_k:

1.i. If the product is positive, it suggests that the presence of J_{k2} amplifies the effect of the linear term $J_{k0} + J_{k1}Q_0$. This implies that the magnitude of the linear estimation of J_k will increase.

1.ii. Conversely, if the product is negative, it implies that J_{k2} dampens or counteracts the effect of the linear term $J_{k0} + J_{k1}Q_0$, resulting in a decrease in the magnitude of the linear estimation of J_k (see Figure 4).

(2) Assessing the joint effects of J_{k0}, J_{k1}, and J_{k2} through the product $J_{k0}J_{k1}J_{k2}$:

2.i. This product considers the interaction between all three coefficients J_{k0}, J_{k1}, and J_{k2}. If the product is positive, it indicates a reinforcement of the flux J_k by J_{k2}, leading to an increase in the magnitude of J_k. Conversely, a negative product suggests a damping effect on $|J_k|$ due to the combined influence of J_{k0}, J_{k1}, and J_{k2} (see Figure 5).

(3) Computing the product $J_{k0}(J_{k1} + J_{k2}Q_0)$ to observe the effects of small Q_0 on J_k:

3.i. If the product is positive (negative), it indicates that a small positive Q_0 will enhance (diminish) $|J_k|$. However, since this scenario is akin to computing the product $J_{k0}J_{k1}$ in the previous section where Q_0 is small, it can be disregarded.

In the subsequent discussion, we will review the aforementioned cases. However, prior to that, we utilize Figure 3 to showcase the transformative impacts of introducing the Q_0^2 term, transitioning the behavior from linear to nonlinear (quadratic).

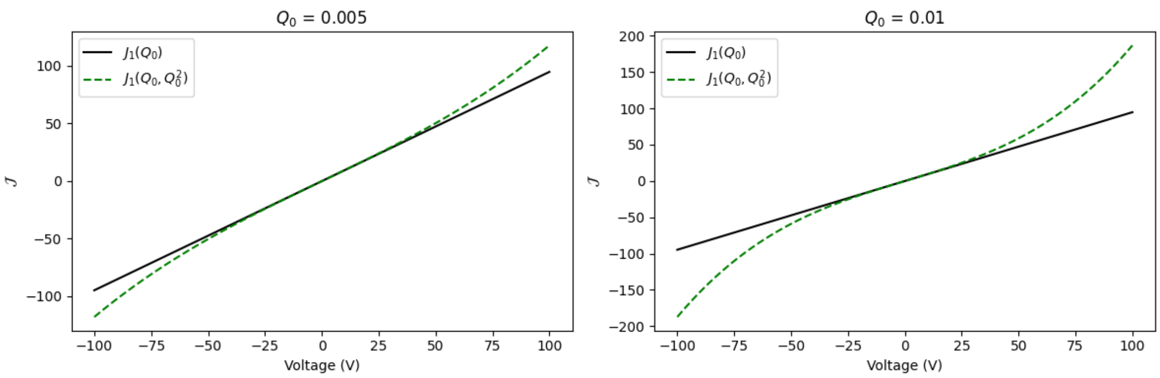

Figure 3. Linear ($J_1(Q_0) = J_{10} + J_{11}Q_0$) and quadratic ($J_1(Q_0) = J_{10} + J_{11}Q_0 + J_{12}Q_0^2$) approximations of flux J_1 for boundary concentrations $L = 0.9, R = 1$.

Figure 3 illustrates that, transitioning from linear to quadratic, the sign of the flux J_1 never changes in the observed cases, as expected, while the magnitude of J_1 increases. However, this method has several limitations: its primary constraint is its representation of only specific cases, which may not be indicative of other scenarios. Furthermore, despite providing similar figures, descerning whether the quadratic term diminishes or amplifies the flux remains challenging. Another limitation is its inability to clearly illustrate how the flux behaves for very small values of V.

4.2.1. Exploring the influence of J_{k2} on the magnitude of linear estimation of the flux J_k

In this section, we delve into the intricate relationship between the second order flux component, J_{k2}, and the linear estimation of flux J_k, where $k = 1, 2$. Given that $J_k \approx J_{k0} + J_{k1}Q_0$, we examine the influence of the second order flux, J_{k2}, on the flux J_k for $k = 1, 2$ by analyzing its effects on the linear estimate of J_k. To initiate our exploration, we construct plots of the product $(J_{k0} + J_{k1}Q_0)J_{k2}$, which effectively illustrates the impact of the second order flux J_{k2} on the linear approximation of J_k. Referencing Figure 4 specifically enables a visual comprehension of these effects for both $k = 1$ and $k = 2$ scenarios.

We emphasize that due to the smallness of Q_0, the term J_{k1} could be ignored, facilitating a direct calculation of $J_{k0}J_{k2}$ to evaluate the influence of J_{k2} on the linear approximation magnitude of J_k, yielding the same results.

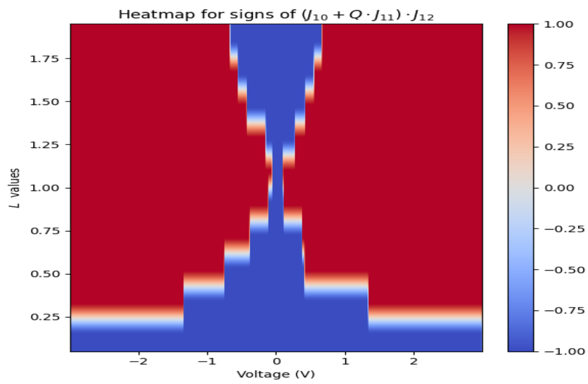

Figure 4. Heatmap depicting $(J_{10} + Q_0J_{11})J_{12}$ with $Q_0 = 0.01$, while varying concentration L from zero to two and keeping concentration R fixed at 1.

The following insights are obtained from numerical observations:

(a) When the left and right boundary concentrations (L and R, respectively) are almost equal ($L \approx R$), a small positive Q_0 increases the magnitude of linear estimations for both J_1 and J_2. This trend is highlighted by the red region near $L = 1$ in Figure 4.

(b) In cases when the boundary concentrations are unequal, denoted as $L \neq R$, two critical voltages V_1^* and V_2^* emerge:

b.i. For voltages V within the range (V_1^*, V_2^*), a small positive Q_0 reduces the magnitude of linear estimations for both J_1 and J_2.

b.ii. Conversely, for voltages V outside the range V_1^* to V_2^*, i.e., for $V < V_1^*$ or $V > V_2^*$, a small positive Q_0 increases the magnitude of linear estimations for both J_1 and J_2.

Furthermore, as the difference between L and R increases, the voltage ranges where a small positive Q_0 reduces the magnitude of linear estimations for both J_1 and J_2 also expand.

4.2.2. Evaluating the combined impact of J_{10}, J_{11}, and J_{12} through their product

In this part, we explore the combined impact of J_{10}, J_{11}, and J_{12} by examining their product, $J_{10}J_{11}J_{12}$. This product captures the interplay among all three coefficients: J_{k0}, J_{k1}, and J_{k2}. A positive product signifies a reinforcement of the flux J_k, resulting in an amplified magnitude of J_k. Conversely, a negative product indicates a damping effect on $|J_k|$, reflecting the combined influence of J_{k0}, J_{k1}, and J_{k2}.

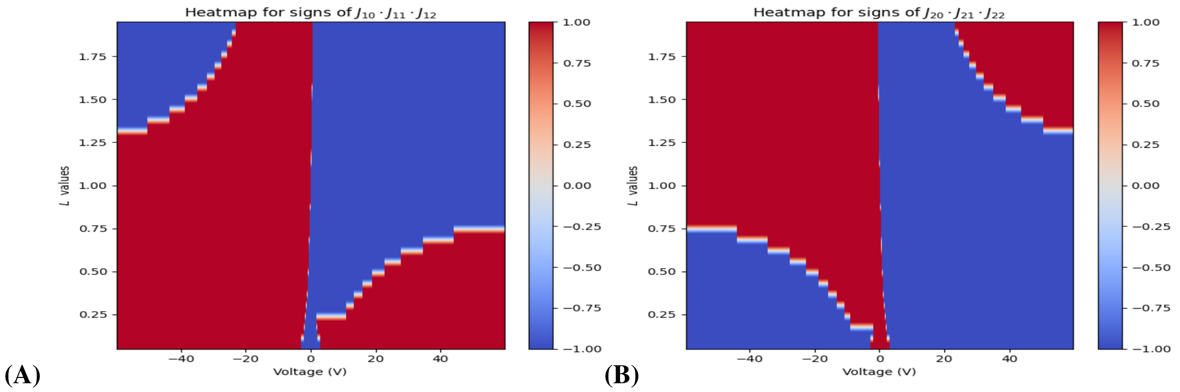

Figure 5. Visualization of heatmaps illustrating sign agreement for the products $J_{10}J_{11}J_{12}$ (panel A) and $J_{20}J_{21}J_{22}$ (panel B). Concentration L varies from zero to two while R is fixed at 1, shedding light on the impact of linear terms.

The observations can be summarized as follows:

(a) When the left and right boundary concentrations are in proximity (i.e., $L \approx R$), there exists a single critical value $V_0^* \approx 0$. Under this condition:

a.i. If $V > V_0^*$, then $J_{k0}J_{k1}J_{k2} < 0$, leading to a damping effect on $|J_k|$ for $k = 1, 2$.

a.ii. If $V < V_0^*$, then $J_{k0}J_{k1}J_{k2} > 0$, resulting in an amplified effect on $|J_k|$ for $k = 1, 2$. (Refer to Figure 5 near $L = 1$.)

(b) Conversely, when the left and right boundary concentrations are not sufficiently close, there are two critical voltages: one is $V_0^* \approx 0$, and the other could be either $V_-^* < 0$ or $V_+^* > 0$, depending on the channel geometry and boundary concentration values. Under these conditions:

b.i. If V_0^* and V_-^* are the critical values, then for V in the interval (V_-^*, V_0^*), $J_{k0}J_{k1}J_{k2} > 0$, leading to an increasing $|J_k|$, and for V outside this interval, $J_{k0}J_{k1}J_{k2} < 0$, resulting in a diminishing effect on $|J_k|$.

b.ii. However, if V_0^* and V_+^* are the critical values, then for V in the interval (V_0^*, V_+^*), $J_{k0}J_{k1}J_{k2} < 0$, causing decreasing of $|J_k|$, and for V outside this interval, $J_{k0}J_{k1}J_{k2} > 0$, leading to a strengthened effect on $|J_k|$.

Additionally, as the disparity between L and R widens, the two critical voltages converge (refer to Figure 5 far from $L = 1$).

4.3. Estimating errors and assessing nonlinear effects for fluxes

In the context of Taylor expansions and polynomial approximations, error estimation serves to assess the impact of truncating the series at a finite order. Neglecting higher-order terms in the expansion introduces approximation errors, which can lead to deviations from the true function behavior. Therefore, quantifying these errors is essential for ensuring the validity of the approximation and understanding its limitations. We explore the calculation and analysis of approximation errors introduced by neglecting higher-order terms in the expansion. By examining the magnitude and significance of these errors, we gain insights into the accuracy of the approximations and the necessity of including additional terms in the expansion.

We present a detailed methodology for computing and analyzing approximation errors in the context of Taylor expansions. This involves calculating the error term introduced by neglecting the J_{12} and J_{22} terms in the Taylor expansion:

$$\text{Error Estimate for } J_1 = (J_{10} + J_{11}Q_0 + J_{22}Q_0^2) - (J_{10} + J_{11}Q_0) = J_{12}Q_0^2.$$

This error estimation evaluates the approximate value missed by fluxes when using the linear term. In other words, incorporating $J_{12}Q_0^2$ allows us to approach the exact value of flux J_1, while omitting it provides an estimation of the error. Similarly, this applies to flux J_2 and the term $J_{22}Q_0^2$. Since Q_0 is small, Q_0^2 and, consequently, $J_{12}Q_0^2$ are also small. Therefore, we primarily focus on its sign to determine if flux J_1 gains a small value (if J_{12} is positive) or misses a small value (if J_{12} is negative). Figure 6(A) demonstrates that for a fixed R, there exists a voltage V_L for any L, such that for $V < V_L$, flux J_1 misses, and for $V > V_L$, it gains a small value when the approximation becomes more accurate by adding the nonlinear term J_{12}. Similarly, for J_2, Figure 6(B) indicates that for a fixed R, there exists a voltage V_L (same as for J_1) for any L, such that for $V < V_L$, flux J_2 gains, and for $V > V_L$, it misses a small value when the approximation becomes more accurate by adding the nonlinear term J_{22}. It is important to note that L and R are independent here; thus, if one fixes L, and varies R, a similar discussion applies (refer to the figures available in the GitHub repository).

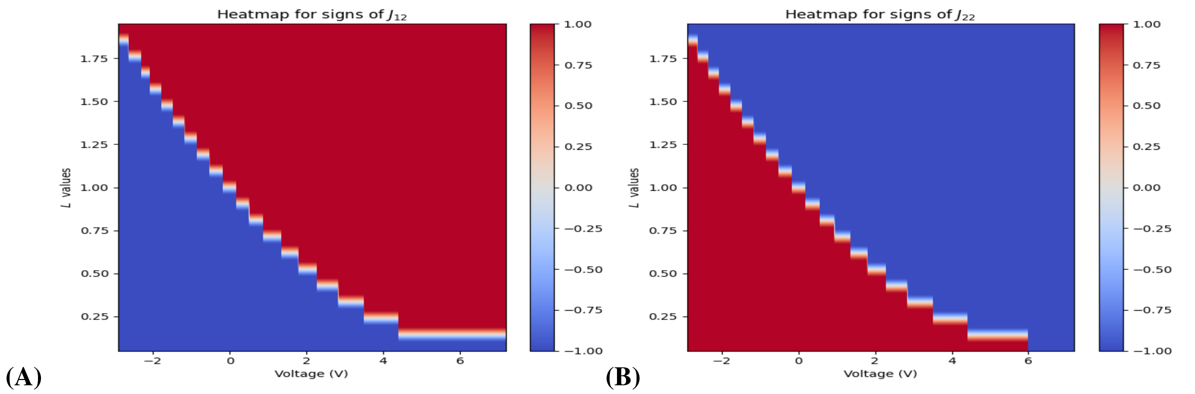

Figure 6. Heatmaps for J_{12} and J_{22} with varying concentration L from zero to two and fixed concentration $R = 1$.

Nevertheless, error estimation in Taylor expansions is not without its challenges. One significant challenge lies in finding the exact solution against which to compare the approximated results. In many cases, the exact solution may be unknown or difficult to determine, leading to uncertainties in the accuracy of the error estimation. Additionally, the choice of expansion point in the Taylor series can significantly impact the magnitude and behavior of the error. Moreover, there exists a trade-off between accuracy and computational cost when considering the inclusion of higher-order terms in the expansion. While including more terms may improve the accuracy of the approximation, it also increases the computational complexity and resource requirements. Acknowledging these obstacles underscores the complexity and uncertainty inherent in error estimation methods and highlights the need for further research to address these limitations and enhance the reliability of numerical approximations.

4.4. *Impact of higher-order solutions on the I-V relation*

This section explores the impact of permanent charge on the current-voltage (I-V) relationship. We investigate how the presence of permanent charge influences the electrical behavior of the system. By examining the influence of permanent charge on electrical behavior, a deeper understanding of the underlying mechanisms governing charge transport and device performance is sought.

In Section 4.4 of [16], an analysis of the impact of small permanent charges Q_0 on I-V relations was conducted, specifically focusing on the zeroth and first-order terms of Q_0. Here, we present some of their findings concerning equal diffusion coefficients and subsequently validate these results through our numerical investigations. Furthermore, we extend the inquiry to higher orders and explore the influence of the second order terms in permanent charge Q_0 on the I-V relation.

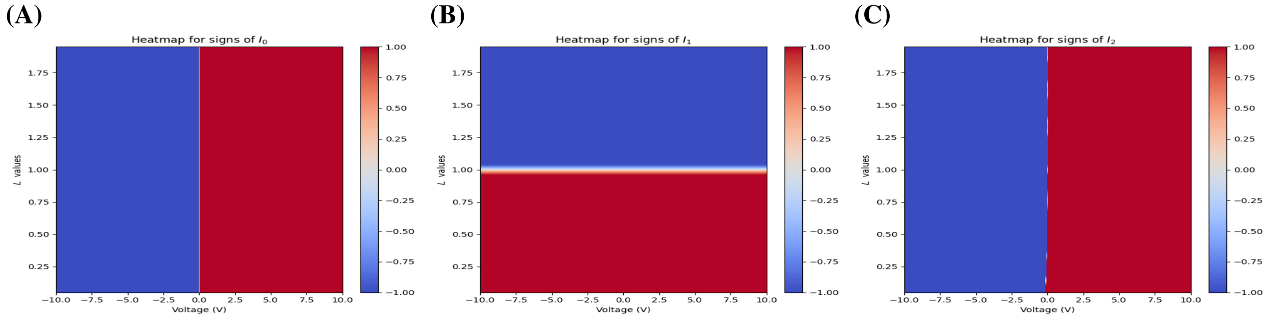

Figure 7. Heatmaps for I_0 (panel A), I_1 (panel B) and I_2 (panel C), versus V, with varying concentration L from zero to two and fixed concentration $R = 1$.

The authors of [16] demonstrated that the current I_0 remains unaffected by boundary concentrations, while I_1 does depend on them. Specifically, they established the existence of a V_{rev} (which equals zero when the diffusion coefficients D_i's are equal) where $I_0 < 0$ if $V < V_{rev}$ and $I_0 < 0$ if $V > V_{rev}$, irrespective of L and R values. This finding aligns with our numerical investigations depicted in Figure 7(A). It is worth noting that when $V_{rev} = 0$ (for equal diffusion coefficients), the righthand sides of Figure 7(A) are red, indicating $I_0 > 0$ for $V > V_{rev} = 0$, and the left-hand side is blue, indicating $I_0 < 0$ for $V < V_{rev} = 0$, regardless of L and R values.

Additionally, Theorem 4.14 in [16] asserts that I_1 does vary with L and R; specifically, for equal diffusion coefficients, $I_1 > 0$ when $L < R$ and $I_0 < 0$ when $L > R$. This result is also consistent with our numerical investigations shown in Figure 7(B) where $R = 1$ is fixed. The lower part of the figure, representing $L < R$, is red, indicating $I_1 > 0$, while the upper part, where $L > R$, is blue, indicating $I_1 < 0$ in this scenario.

Remark 4.5. *In [16], it is additionally shown how the current I_1 is influenced by the boundary V (in* *addition to L and R) for nonequal diffusion coefficients. Nevertheless, we chose not to delve into the numerical results for this scenario in order to maintain our primary focus on the higher-order terms involving the permanent charge Q_0 and its impact on the I-V relation.*

We now expand upon the findings regarding the second order terms of Q_0 using numerical analysis, as depicted in Figure 7(C). These investigations reveal that, akin to I_0, the current I_2 remains unaffected by the boundary concentrations L and R but is contingent solely upon the boundary V, which equals zero when diffusion coefficients are equal. Consequently, we derive the following relationship:

$$I_2 > 0 \ \text{ for } \ V > 0, \quad \text{and} \quad I_2 < 0 \ \text{ for } \ V < 0. \tag{4.2}$$

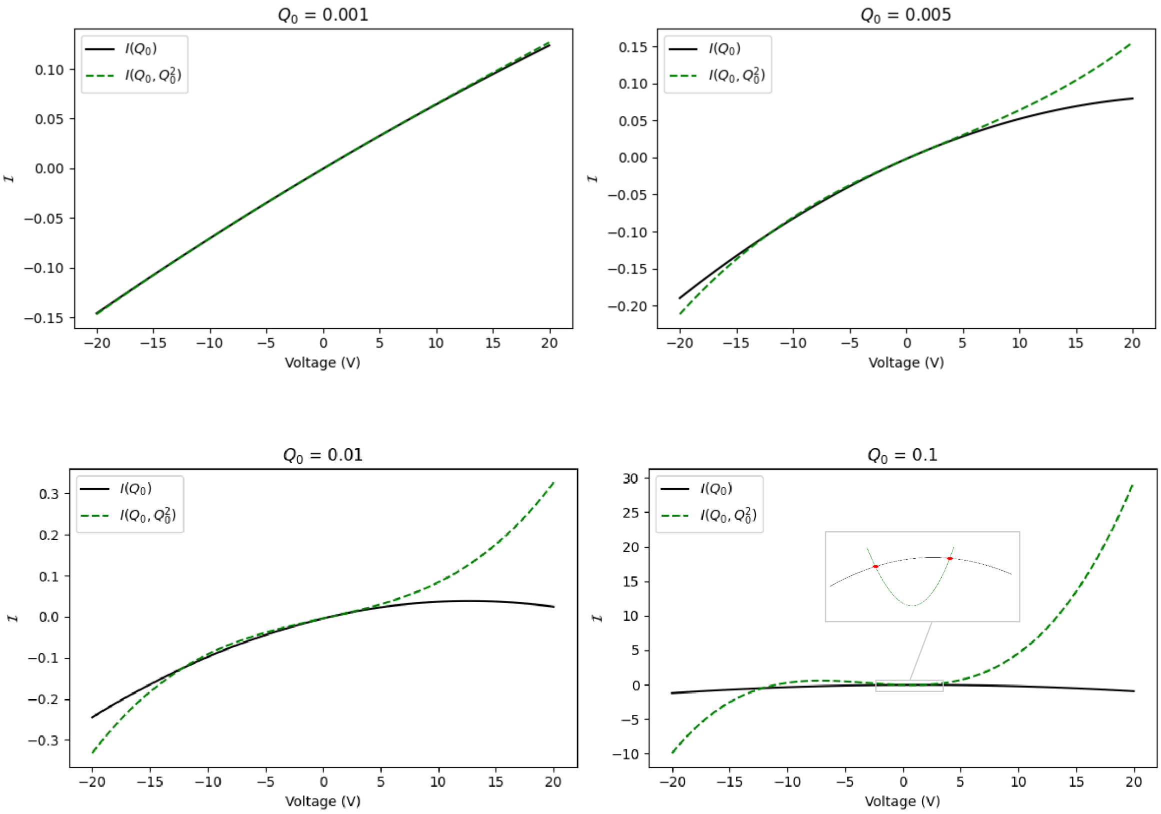

Figure 8. Linear ($J_1(Q_0) = J_{10} + J_{11}Q_0$) (represented by solid black curves) and quadratic ($J_1(Q_0) = J_{10} + J_{11}Q_0 + J_{12}Q_0^2$) (represented by dashed green curves) approximations of the current $\mathcal{I}$ with respect to V for various fixed values of $Q_0 = 0.001, 0.005, 0.01, 0.1$ and boundary concentrations $L = 0.008, R = 0.001$.

Remark 4.6. *It is noteworthy to mention that in Eq (4.2), we could potentially assert* $V > V_{rev} = 0$ *(and similarly for the converse case).*

In the following discussion, we employ Figures 8 and 9 (for fixed boundary concentrations at $L = 0.008, R = 0.001$, while varying Q_0 and V) to illustrate the significant effects of introducing the Q_0^2 term, which leads to a transition in behavior from linear to nonlinear (quadratic). Several key observations from these figures are outlined below:

(a) **Monotonicity in V for small Q_0 and non-monotonic behavior in Q_0 for fixed V:** Observing Figure 8, we note that for small Q_0, the current $\mathcal{I}$ shows a monotone (increasing) behavior with respect to V. This aligns with the expectation that the current is primarily influenced by V when Q_0 is small. However, as depicted in Figure 9, monotonicity does not hold concerning Q_0 when V is held constant.

(b) **Bifurcations of $\mathcal{I} = 0$ (reversal potential):** For values of Q_0 near $Q_0 = 0.1$, as depicted in Figure 8, the second-order solution in terms of Q_0 for the current, $\mathcal{I}$, appears to have three roots. This phenomenon was not anticipated or predicted in earlier studies such as those mentioned in [16, 54].

(c) Figure 8 ($Q_0 = 0.1$) shows that the dashed green curve for the quadratic current solution lies below the linear solution between two red circles representing negative and positive voltages. This indicates that a small positive Q_0 may increase or decrease the magnitude of linear current estimations.

5. Permanent charge effects on flux ratios

This section delves into the influence of a positive permanent charge on the fluxes of both cation and anion species. To quantify this influence, we introduce the flux ratio $\lambda_k(Q_0) = J_k(Q_0)/J_k(0)$, which compares the flux $J_k(Q_0)$ associated with a permanent charge Q_0 to the flux $J_k(0)$ with zero permanent charge, for a given ion species under specific boundary conditions and channel geometry. Note that in the following, we may use $\lambda_k(Q_0)$, $\lambda_k(Q_0, V)$, or $\lambda_k(Q_0, Q_0^2)$ for simplicity or to demonstrate the dependence of flux ratios on V or Q_0^2, respectively.

For $n = 2$ with $z_1 = 1$ and $z_2 = -1$, detailed analysis of the impact of permanent charge described by Eq (2.9) on flux ratios has been conducted for both small and large Q_0 [16,27,36]. The flux ratio $\lambda_k(Q_0)$ serves as a metric for measuring the impact of the permanent charge Q_0: When $\lambda_k(Q_0) > 1$, the flux is augmented by Q_0, and when $\lambda_k(Q_0) < 1$, the flux is diminished by Q_0. An analysis of PNP models governing ionic flows reveals a universal principle regarding the effects of permanent charge [27]:

Proposition 5.1. *For a positive permanent charge Q_0, if $\lambda_1(Q_0)$ denotes the flux ratio for cation species and $\lambda_2(Q_0)$ signifies the flux ratio for anion species, then $\lambda_1(Q_0) < \lambda_2(Q_0)$ holds true irrespective of boundary conditions and channel geometry.*

This proposition is precise in that, especially for a small positive Q_0, various scenarios emerge based on boundary conditions and channel geometry, such as (*i*) $\lambda_1(Q_0) < 1 < \lambda_2(Q_0)$, (*ii*) $1 < \lambda_1(Q_0) < \lambda_2(Q_0)$, and (*iii*) $\lambda_1(Q_0) < \lambda_2(Q_0) < 1$. Each of these options captures unique details in how flux ratios change with a positive permanent charge.

In the preceding section, we generated heatmaps to visualize flux sign patterns across various figures in our investigations, necessitating the identification of roots within the expressions. However, due to the computational complexity involved, not all initial values are conductive to heatmap creation. The extensive computations introduce numerous tiny errors across a range of values, ultimately resulting in significant final errors in the output, thus reducing the effectiveness of heatmaps for representation. Consequently, we refrain from employing heatmaps in the subsequent section and instead focus on specific cases to derive results.

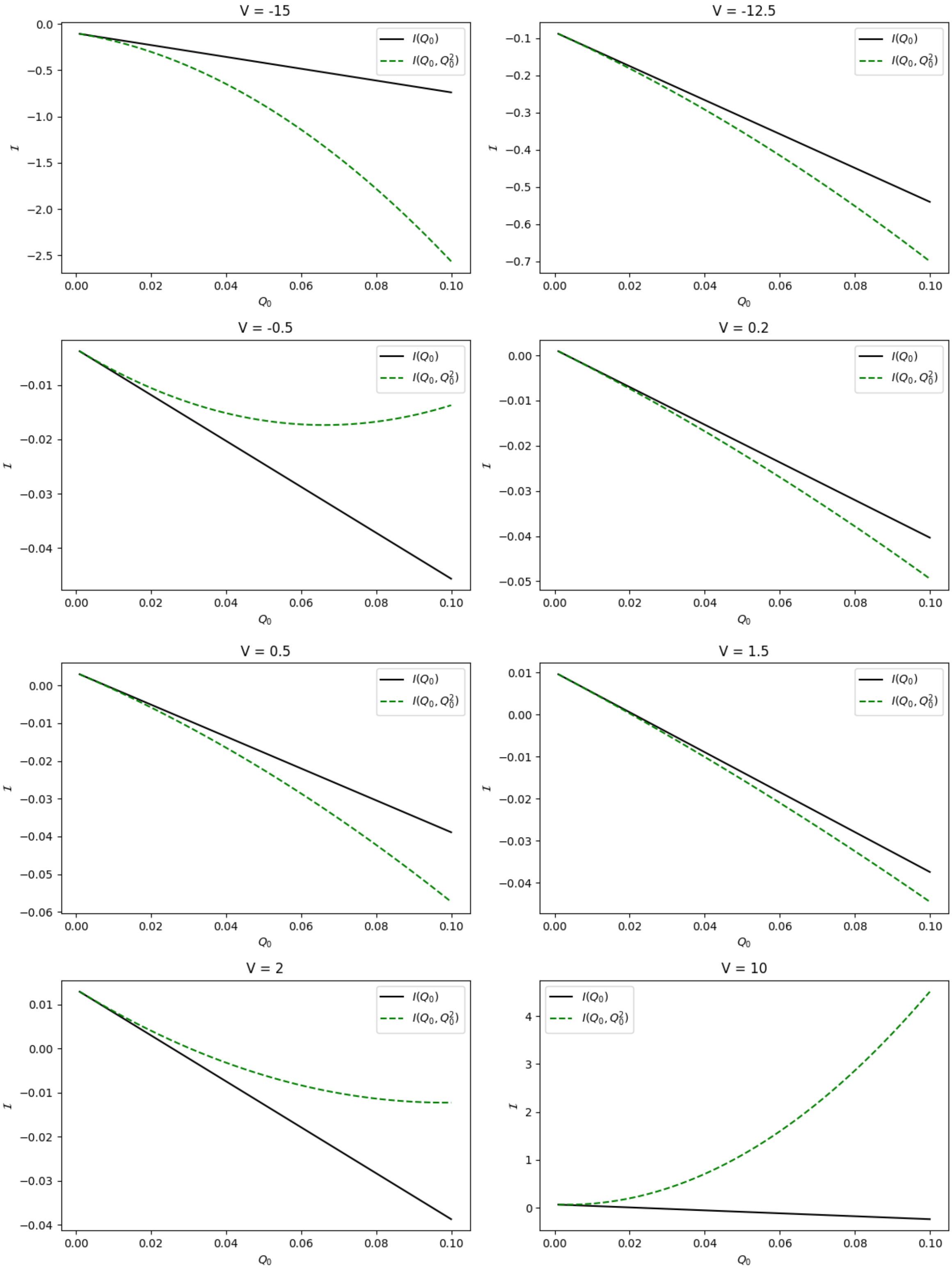

Figure 9. *Linear ($J_1(Q_0) = J_{10} + J_{11}Q_0$) approximations (solid black curves) and quadratic ($J_1(Q_0) = J_{10} + J_{11}Q_0 + J_{12}Q_0^2$) approximations (dashed green curves) of the current $\mathcal{I}$ with respect to Q_0 for various fixed values of $V = -15, -12.5, -0.5, 0.2, 0.5, 1.5, 2, 10$ and boundary concentrations $L = 0.008, R = 0.001$.*

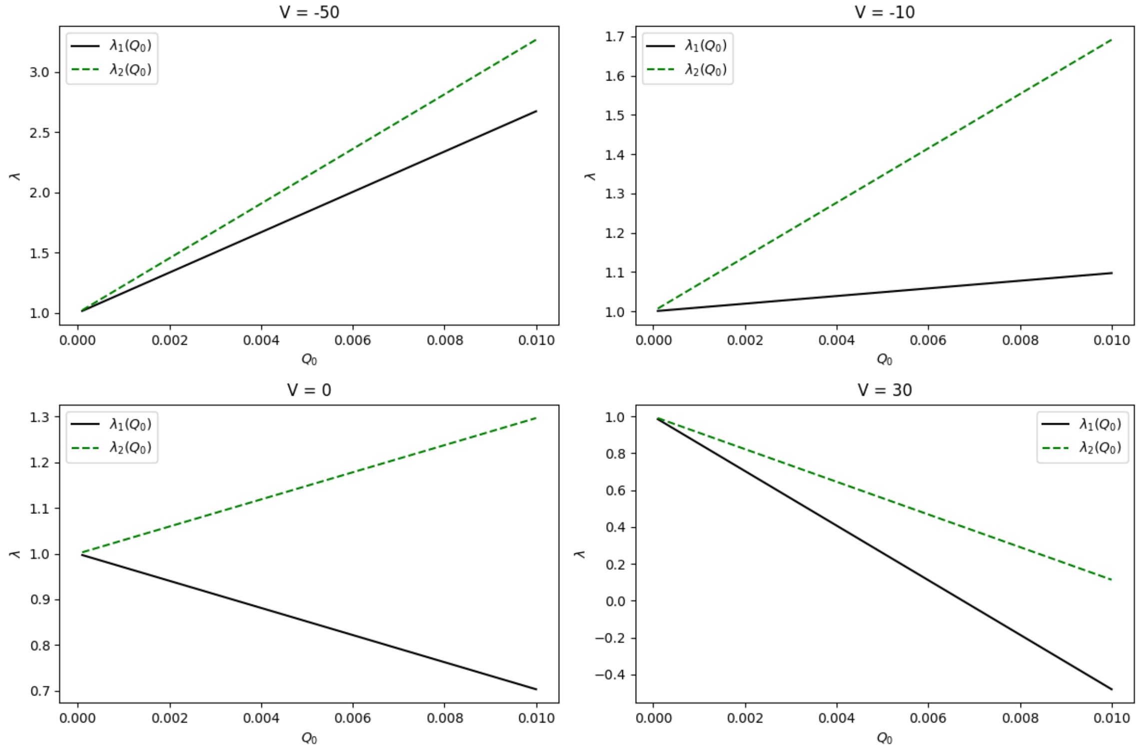

(a) Linear approximations.

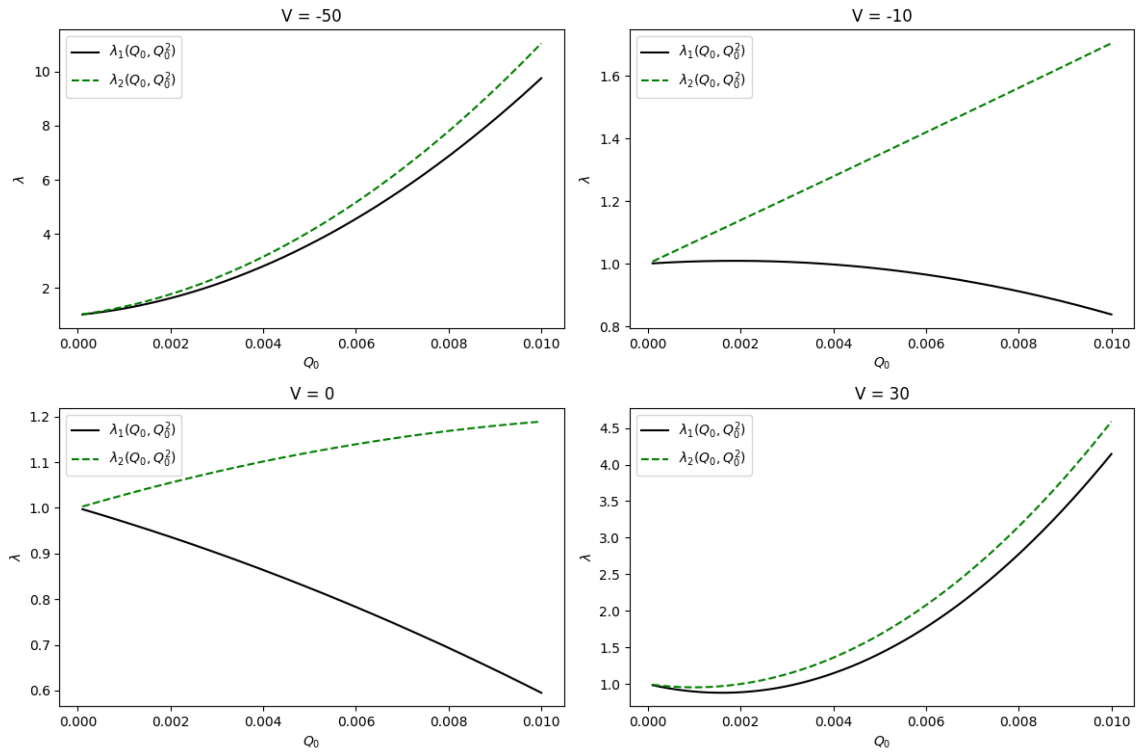

(b) Quadratic approximations.

Figure 10. Linear (a) and quadratic (b) approximations of the flux ratios λ_1 (solid black lines) and λ_2 (dashed green lines) with respect to Q_0, considering various fixed values of $V = -50, -10, 0, 30$, and $L = 0.008, R = 0.001$.

5.1. *Dependence of flux ratios on Q_0 for fixed V*

For small Q_0, as V increases, the change occurs from $1 < \lambda_1 < \lambda_2$ to $\lambda_1 < 1 < \lambda_2$ and to $\lambda_1 < \lambda_2 < 1$ or from $\lambda_1 < \lambda_2 < 1$ to $\lambda_1 < 1 < \lambda_2$ and to $1 < \lambda_1 < \lambda_2$ (refer to [54]).

(i) **Non-monotonic behavior in Q_0 for fixed values of V:** Examining Figure 10 for $V = -10$ (and similarly for $V = 30$), it becomes apparent that while the flux ratio λ_2 appears to increase (or decrease) based on linear estimates, the quadratic approximations reveal a different trend.

(ii) **Possible Pitchfork Bifurcations at $\lambda_k = 1$:** In Figure 10 (for $V = 30$), the behavior of $\lambda_k(Q_0, Q_0^2)$ for various Q_0 values, influenced by second-order solutions in Q_0, exhibits non-monotonic trends and can cross the value of 1 twice. This implies the existence of two instances where $\lambda_k(Q_0, Q_0^2) = 1$, or there is a Q_0^* for which $\frac{\partial \lambda_k}{\partial V}(Q_0^*, V) = 0$, indicating the possibility of bifurcations at $\lambda_k(Q_0^*, V) = 1$. As we will see in Section 5.2 (part ii), there is a V^* such that $\frac{\partial \lambda_k}{\partial V}(Q_0, V^*) = 0$. Consequently, there is a chance that the corresponding value of Q_0 for which $\frac{\partial \lambda_k}{\partial V}(Q_0, V^*) = 0$ is precisely Q_0^*. This implies the existence of (Q_0^*, V^*) such that $\frac{\partial \lambda_k}{\partial V}(Q_0^*, V^*) = \frac{\partial \lambda_k}{\partial Q_0}(Q_0^*, V^*) = 0$, potentially leading to a pitchfork bifurcation.

5.2. *Dependence of flux ratios on V for fixed permanent charges*

We now examine the dependence of ion fluxes λ_1 and λ_2 on V for several fixed values of Q_0. In Figure 11, they are plotted as functions of $V \in (-50, 50)$ for $Q_0 = 0.001, 0.005$, and 0.01.

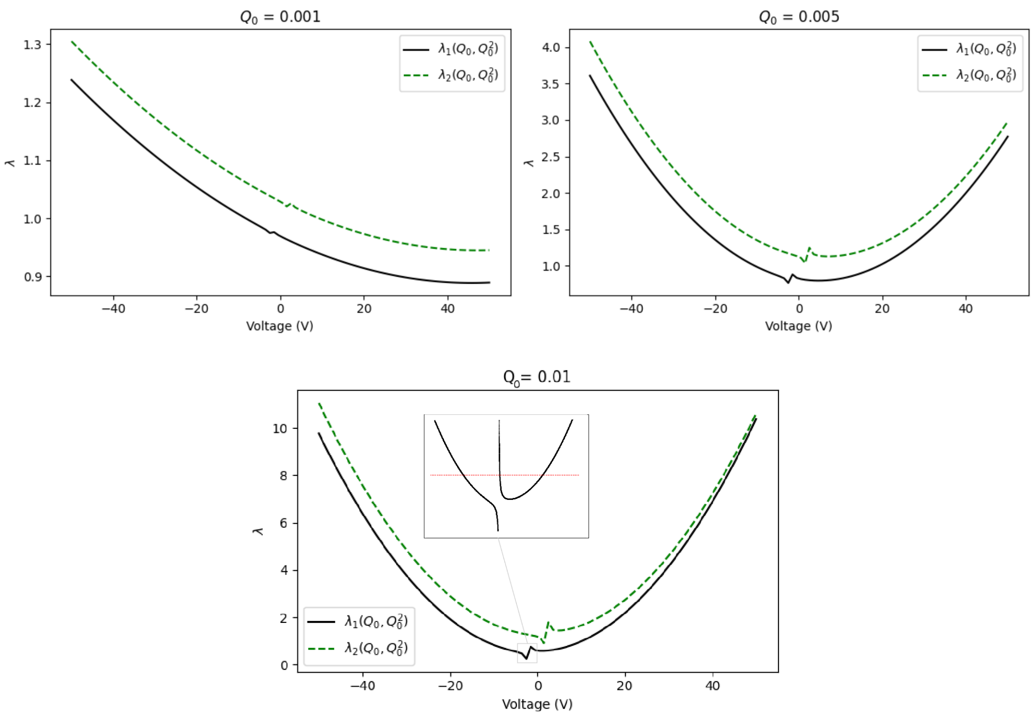

Figure 11. Quadratic approximations of the flux ratios λ_1 (solid black lines) and λ_2 (dashed green lines) with respect to V, considering various fixed values of $Q_0 = 0.001, 0.005, 0.01$, and $L = 0.008, R = 0.001$. The horizontal red line in the zoomed-in image is $\lambda = 1$ that shows there are three voltage values for which the flux ratio λ_1 becomes one and this is bifurcation.

(i) **Monotonicity in V for small Q_0.** From Figure 11, one observes that for very small $Q_0 = 0.001$, both λ_1 and λ_2 are monotone (decreasing) in V. This is consistent with the theoretical prediction made in [16] and also with the numerical observations in [54], and with the intuition that the flux ratios are dominated by the effects of V when Q_0 is small.

(ii) **Bifurcations at $\lambda_k = 1$:** In Figure 11, for various Q_0 values, $\lambda_1(Q_0, Q_0^2)$, influenced by second-order solutions in Q_0, exhibits a discontinuity near $\lambda_1 = 1$, resulting in three values where $\lambda_1 = 1$. Additionally, with increasing Q_0, fluxes show non-monotonic behavior in V, crossing $\lambda_1 = 1$ multiple times. These behaviors were not predicted by the analysis in [16], but non-monotonicity was discussed in [54] through numerical observations. Similar discussions apply to $\lambda_2 = 1$.

6. Concluding remarks and future work

In this study, we presented a comprehensive exploration of ion channel dynamics, focusing on the intricate influence of permanent charges. Theoretical and numerical analyses have been combined to unveil the qualitative shifts in fluxes, flux ratios, and electric potentials at higher-order contributions of permanent charge. The investigation has delved into the subtle interplay between boundary conditions and channel geometry, elucidating the nuanced impact of permanent charges on ion channel behavior. Our findings contribute to the understanding of ion electro-diffusion, shedding light on the complex interactions that arise due to permanent charges. The systematic perturbation analysis, spanning zeroth, first, and second order solutions, has provided valuable insights into the behavior of the system under the influence of small permanent charges. As we conclude this study, avenues for further research emerge.

As indicated in Remark 4.1, the complexity of the quadratic solutions in Section 3.2 led us to utilize numerical observations to further explore the second-order solutions and their effects on the system. Integrating numerical observations with analytical insights improves our understanding of the analytical results, which we plan to continue studying in the future. Additionally, the application of advanced numerical techniques and simulations may offer a more detailed understanding of ion channel behavior in complex biological environments. Further investigations could also delve into the impact of permanent charges on specific ion channel types, allowing for a more targeted analysis of their behavior. Moreover, experimental validation and comparison with existing biological data would provide a bridge between theoretical insights and real-world observations, enhancing the practical relevance of our findings.

Exploring local hard-sphere PNP systems, which account for finite ion sizes, offers valuable insights into the dynamics of ionic channels by considering ion sizes d [53]. However, the computations become more complex in this case. A fascinating aspect of this study involves investigating higher-order solutions concerning ion size d and permanent charge Q_0, specifically deriving Q_0^2, $Q_0 d$, and d^2 solutions. We derived solutions involving Q_0^2 in this manuscript. The work presented in [25] delves into the higher-order effects of ion size and provides d^2 solutions. Additionally, the paper [53] examines PNP models with ion size and permanent charge, and to complete the puzzle, one must carefully derive $Q_0 d$ terms from that paper. By assembling all these quadratic terms, a more accurate exploration of the higher-order impacts of ion size and permanent charge becomes possible.

Use of AI tools declaration

The authors declare they have not used Artificial Intelligence (AI) tools in the creation of this article.

Acknowledgments

The author acknowledges the valuable comments and support provided by Weishi Liu from the University of Kansas, Bob Eisenberg from Rush University Medical Center, and Mingji Zhang from New Mexico Tech University. Additionally, the author expresses gratitude for the valuable comments and support received from the anonymous reviewers.

Conflict of interest

The author declares there is no conflict of interest.

References

1. D. Boda, W. Nonner, M. Valisko, D. Henderson, B. Eisenberg, D. Gillespie, Steric selectivity in Na channels arising from protein polarization and mobile side chains, *Biophys. J.*, **93** (2007), 1960–1980. https://doi.org/10.1529/biophysj.107.105478
2. B. Hille, *Ion Channels of Excitable Membranes*, 3rd Edition, Sinauer Associates, Inc., Sunderland, Massachusetts, USA, 2001.
3. B. Eisenberg, Ion channels as devices, *J. Comput. Electron.*, **2** (2003), 245–249. https://doi.org/10.1023/B:JCEL.0000011432.03832.22
4. B. Eisenberg, Proteins, channels, and crowded ions, *Biophys. Chem.*, **100** (2003), 507–517. https://doi.org/10.1016/S0301-4622(02)00302-2
5. A. L. Hodgkin, A. F. Huxley, A quantitative description of membrane current and its application to conduction and excitation in nerve, *J. Physiol.*, **117** (1952), 500–544. https://doi.org/10.1113/jphysiol.1952.sp004764
6. A. L. Hodgkin, R. D. Keynes, The potassium permeability of a giant nerve fibre, *J. Physiol.*, **128** (1955), 61–88. https://doi.org/10.1113/jphysiol.1955.sp005291
7. A. Malasics, D. Gillespie, W. Nonner, D. Henderson, B. Eisenberg, D. Boda, Protein structure and ionic selectivity in calcium channels: Selectivity filter size, not shape, matters, Biochim, *J. Biophys. Acta*, **1788** (2009), 2471–2480. https://doi.org/10.1016/j.bbamem.2009.09.022
8. A. L. Hodgkin, A. F. Huxley, Currents carried by sodium and potassium ions through the membrane of the giant axon of *Loligo*, *J. Physol.*, **116** (1952), 449–472. https://doi.org/10.1113/jphysiol.1952.sp004717
9. A. L. Hodgkin, A. F. Huxley, The components of membrane conductance in the giant axon of *Loligo*, *J. Physiol.*, **116** (1952), 473–496. https://doi.org/10.1113/jphysiol.1952.sp004718
10. S. Ji, B. Eisenberg, W. Liu, Flux ratios and channel structures, *J. Dyn. Differ. Equations*, **31** (2019), 1141–1183. https://doi.org/10.1007/s10884-017-9607-1

11. X. Deng, Y. Jia, M. Zhang, Studies on current-voltage relations via Poisson-Nernst-Planck systems with multiple cations and small permanent charges, *J. Appl. Anal. Comput.*, **12** (2022), 932–951. https://doi.org/10.11948/20210003

12. Y. Wang, L. Zhang, M. Zhang, Mathematical analysis on current-voltage relations via classical Poisson-Nernst-Planck systems with nonzero permanent charges under relaxed electroneutrality boundary conditions, *Membranes*, **13** (2023), 131. https://doi.org/10.3390/membranes13020131

13. J. Chen, Y. Wang, L. Zhang, M. Zhang, Mathematical analysis of Poisson-Nernst-Planck models with permanent charges and boundary layers: studies on individual fluxes, *Nonlinearity*, **34** (2021), 3879–3906. https://doi.org/10.1088/1361-6544/abf33a

14. B. Eisenberg, W. Liu, Poisson-Nernst-Planck systems for ion channels with permanent charges, *SIAM J. Math. Anal.*, **38** (2007), 1932–1966. https://doi.org/10.1137/060657480

15. B. Eisenberg, W. Liu, H. Xu, Reversal permanent charge and reversal potential: Case studies via classical Poisson-Nernst-Planck models, *Nonlinearity*, **28** (2015), 103–128. https://doi.org/10.1088/0951-7715/28/1/103

16. S. Ji, W. Liu, M. Zhang, Effects of (small) permanent charge and channel geometry on ionic flows via classical Poisson-Nernst-Planck models, *SIAM J. Appl. Math.*, **75** (2015), 114–135. https://doi.org/10.1137/140992527

17. W. Liu, Geometric singular perturbation approach to steady-state Poisson-Nernst-Planck systems, *SIAM J. Appl. Math.*, **65** (2005), 754–766.https://doi.org/10.1137/S0036139903420931

18. W. Liu, One-dimensional steady-state Poisson-Nernst-Planck systems for ion channels with multiple ion species, *J. Differ. Equations*, **246** (2009), 428–451. https://doi.org/10.1016/j.jde.2008.09.010

19. J. K. Park, J. W. Jerome, Qualitative properties of steady-state Poisson-Nernst-Planck systems: Mathematical study, *SIAM J. Appl. Math.*, **57** (1997), 609–630. https://doi.org/10.1137/S0036139995279809

20. M. Zhang, Competition between cations via classical Poisson-Nernst-Planck models with nonzero but small permanent charges, *Membranes*, **11** (2021), 236. https://doi.org/10.3390/membranes11040236

21. M. Zhang, Existence and local uniqueness of classical Poisson-Nernst-Planck systems with multi-component permanent charges and multiple cations, *Discrete Contin. Dyn. Syst. - Ser. S*, **16** (2023), 725–752. https://doi.org/10.3934/dcdss.2022134

22. C. K. R. T. Jones, Geometric singular perturbation theory, in *Dynamical Systems. Lecture Notes in Mathematics*, Springer-Verlag, Berlin, **1609** (1995), 44–118. https://doi.org/10.1007/BFb0095239

23. C. Kuehn, Multiple time scale dynamics, in *Applied Mathematical Sciences*, Springer, Cham, **191** (2015). https://doi.org/10.1007/978-3-319-12316-5

24. R. S. Eisenberg, Atomic biology, electrostatics and ionic channels, in *New Developments and Theoretical Studies of Proteins*, World Scientific, Philadelphia, (1996), 269–357.

25. Y. Fu, W. Liu, H. Mofidi, M. Zhang, Finite ion size effects on ionic flows via Poisson-Nernst-Planck systems: Higher order contributions, *J. Dyn. Differ. Equations*, **35** (2022), 1585–1609. https://doi.org/10.1007/s10884-021-10114-1

26. P. W. Bates, Z. Wen, M. Zhang, Small permanent charge effects on individual fluxes via Poisson-Nernst-Planck models with multiple cations, *J. Nonlinear Sci.*, **31** (2021), 55. https://doi.org/10.1007/s00332-021-09715-3

27. W. Liu, A flux ratio and a universal property of permanent charges effects on fluxes, *Comput. Math. Biophys.*, **6** (2018), 28–40. https://doi.org/10.1515/cmb-2018-0003

28. Z. Wen, P. W. Bates, M. Zhang, Effects on I-V relations from small permanent charge and channel geometry via classical Poisson-Nernst-Planck equations with multiple cations, *Nonlinearity*, **34** (2021), 4464–4502. https://doi.org/10.1088/1361-6544/abfae8

29. B. Eisenberg, W. Liu, H. Mofidi, Effects of diffusion coefficients on reversal potentials in ionic channels, preprint, arXiv:2311.02895.

30. H. Mofidi, Geometric mean of concentrations and reversal permanent charge in Zero-Current ionic flows via Poisson-Nernst-Planck models, preprint, arXiv:2009.09564.

31. H. Mofidi, Reversal permanent charge and concentrations in ionic flows via Poisson-Nernst-Planck models, *Q. Appl. Math.*, **79** (2021), 581–600. https://doi.org/10.1090/qam/1593

32. H. Mofidi, Bifurcation of flux ratio in ionic flows via a PNP model, preprint, arXiv:2311.02895.

33. H. Mofidi, W. Liu, Reversal potential and reversal permanent charge with unequal diffusion coefficients via classical Poisson–Nernst–Planck models, *SIAM J. Appl. Math.*, **80** (2020), 1908–1935. https://doi.org/10.1137/19M1269105

34. W. Liu, X. Tu, M. Zhang, Poisson-Nernst-Planck systems for ion flow with density functional theory for hard-sphere potential: I-V relations and critical potentials. Part II: Numerics, *J. Dyn. Differ. Equations*, **24** (2012), 985–1004. https://doi.org/10.1007/s10884-012-9278-x

35. H. Mofidi, B. Eisenberg, W. Liu, Effects of diffusion coefficients and permanent charge on reversal potentials in ionic channels, *Entropy*, **22** (2020), 325. https://doi.org/10.3390/e22030325

36. L. Zhang, B. Eisenberg, W. Liu, An effect of large permanent charge: Decreasing flu with increasing transmembrane potential, *Eur. Phys. J. Spec. Top.*, **227** (2019), 2575–2601. https://doi.org/10.1140/epjst/e2019-700134-7

37. W. M. Lee, *Python Machine Learning*, John Wiley & Sons, Inc., (2019), 1–296. https://doi.org/10.1002/9781119557500

38. Z. Schuss, B. Nadler, R. S. Eisenberg, Derivation of Poisson and Nernst-Planck equations in a bath and channel from a molecular model, *Phys. Rev. E*, **64** (2001), 1–14. https://doi.org/10.1103/PhysRevE.64.036116

39. V. Barcilon, Ion flow through narrow membrane channels: Part I, *SIAM J. Appl. Math.*, **52** (1992), 1391–1404. https://doi.org/10.1137/0152080

40. Y. Hyon, B. Eisenberg, C. Liu, A mathematical model for the hard sphere repulsion in ionic solutions, *Commun. Math. Sci.*, **9** (2010), 459–475. https://doi.org/10.4310/CMS.2011.v9.n2.a5

41. Y. Hyon, C. Liu, B. Eisenberg, PNP equations with steric effects: A model of ion flow through channels, *J. Phys. Chem.*, **116** (2012), 11422–11441. https://doi.org/10.1021/jp305273n

42. P. M. Biesheuvel, Two-fluid model for the simultaneous flow of colloids and fluids in porous media, *J. Colloid Interface Sci.*, **355** (2011), 389–395. https://doi.org/10.1016/j.jcis.2010.12.006

43. D. Chen, R. Eisenberg, J. Jerome, C. Shu, Hydrodynamic model of temperature change in open ionic channels, *Biophys. J.*, **69** (1995), 2304–2322. https://doi.org/10.1016/S0006-3495(95)80101-3

44. V. Sasidhar, E. Ruckenstein, Electrolyte osmosis through capillaries, *J. Colloid Interface Sci.*, **82** (1981), 1439–1457. https://doi.org/10.1016/0021-9797(81)90386-6

45. R. J. Gross, J. F. Osterle, Membrane transport characteristics of ultra fine capillary, *J. Chem. Phys.*, **49** (1968), 228–234. https://doi.org/10.1063/1.1669814

46. W. Im, B. Roux, Ion permeation and selectivity of OmpF porin: A theoretical study based on molecular dynamics, Brownian dynamics, and continuum electrodiffusion theory, *J. Mol. Biol.*, **322** (2002), 851–869. https://doi.org/10.1016/S0022-2836(02)00778-7

47. B. Roux, T. W. Allen, S. Berneche, W. Im, Theoretical and computational models of biological ion channels, *Q. Rev. Biophys.*, **37** (2004), 15–103. https://doi.org/10.1017/S0033583504003968

48. W. Nonner, R. S. Eisenberg, Ion permeation and glutamate residues linked by Poisson-Nernst-Planck theory in L-type Calcium channels, *Biophys. J.*, **75** (1998), 1287–1305. https://doi.org/10.1016/S0006-3495(98)74048-2

49. W. Liu, B. Wang, Poisson-Nernst-Planck systems for narrow tubular-like membrane channels, *J. Dyn. Differ. Equations*, **22** (2010), 413–437. https://doi.org/10.1007/s10884-010-9186-x

50. Y. Wang, L. Zhang, M. Zhang, Studies on individual fluxes via Poisson-Nernst-Planck models with small permanent charges and partial electroneutrality conditions, *J. Appl. Anal. Comput.*, **12** (2022), 87–105. https://doi.org/10.11948/20210045

51. D. Gillespie, *A Singular Perturbation Analysis of the Poisson-Nernst-Planck System: Applications to Ionic Channels*, Ph.D thesis, Rush University at Chicago, 1999.

52. S. Ji, W. Liu, Poisson-Nernst-Planck systems for ion flow with density functional theory for hard-sphere potential: I-V relations and critical potentials, Part I: Analysis, *J. Dyn. Differ. Equations*, **24** (2012), 955–983. https://doi.org/10.1007/s10884-012-9277-y

53. W. Liu, H. Mofidi, Local Hard-Sphere Poisson-Nernst-Planck models for ionic channels with permanent charges, preprint, arXiv:2203.09113.

54. W. Huang, W. Liu, Y. Yu, Permanent charge effects on ionic flow: a numerical study of flux ratios and their bifurcation, *Commun. Comput. Phys.*, **30** (2021), 486–514. https://doi.org/10.4208/cicp.OA-2020-0057

AIMS Press